Czech Technical University

Faculty of Electrical Engineering
Department of Microelectronics

Diploma thesis

Integrated 8 Channel LAN-WDM Demultiplexer for 400Gbit Ethernet

Integrovaný 8 kanálový LAN-WDM demultiplexer pro 400Gbit Ethernet

Bc. Tomáš Pankrác

Advisor: doc. Ing. Vítězslav Jeřábek, CSc.

2017

ČESKÉ VYSOKÉ UČENÍ TECHNICKÉ V PRAZE

ZADÁNÍ DIPLOMOVÉ PRÁCE

I. OSOBNÍ A STUDIJNÍ ÚDAJE

Příjmení: **Pankrác** Jméno: **Tomáš** Osobní číslo: **392792**

Fakulta/ústav: **Fakulta elektrotechnická**

Zadávající katedra/ústav: **Katedra mikroelektroniky**

Studijní program: **Komunikace, multimédia a elektronika**

Studijní obor: **Elektronika**

II. ÚDAJE K DIPLOMOVÉ PRÁCI

Název diplomové práce:

Integrovaný 8 kanálový LAN-WDM Demultiplexer pro 400 Gbit Ethernet

Název diplomové práce anglicky:

Integrated 8 Channel LAN-WDM Demultiplexer for 400Gbit Ethernet

Pokyny pro vypracování:

1) Seznamte se s problematikou návrhu pasivních optických integrovaných obvodů pro optickou telekomunikaci. Vyberte nejvhodnější řešení pro realizaci 8 kanálové rozbočnice pro 400Gbit Ethernet. Prostudujte metody návrhu a využijte počítačových simulací v programu Lumerical MODE a Solutions. Zhodnoťte dosavadní stav techniky a uveďte motivaci pro vaše řešení.
2) Cílem této práce je navrhnout integrovanou 8 kanálovou optickou rozbočnici, která bude splňovat požadavky standardu LAN-WDM. Návrh musí být realizovatelný běžnými technologiemi Silicon-on-Insulator pro výrobu pasivních optických integrovaných obvodů.
3) Návrh bude ověřen simulacemi v programu Lumerical MODE a Solutions a výsledky porovnány s nyní dostupnými produkty.

Seznam doporučené literatury:

[1] R. Arima, T. Hatano, K. Hiramoto a H. Irie, ?Demonstration of World-First 112 Gbit/s 1310 nm LAN-WDM Optical Transceiver For 100GbE and 100GbE over OTN Applications,? v Optical Fiber Communication Conference, San Diego, California United States, 2010.
[2] W. Shi, X. Wang, C. Lin, H. Yun, Y. Liu, T. Baehr-Jones, M. Hochberg, N. A. F. Jaeger and L. Chrostowski, 'Silicon photonic grating-assisted, contra-directional couplers,' OPTICS EXPRESS, pp. 1-18, 5 February 2013.
[3] Okamoto K. : Fundamentals of Optical Waveguides, Academic Press, USA, 2006

Jméno a pracoviště vedoucí(ho) diplomové práce:

doc. Ing. Vítězslav Jeřábek CSc., katedra mikroelektroniky FEL

Jméno a pracoviště druhé(ho) vedoucí(ho) nebo konzultanta(ky) diplomové práce:

Datum zadání diplomové práce: **30.03.2017** Termín odevzdání diplomové práce: _____

Platnost zadání diplomové práce: [redacted]

[redacted] [redacted] [redacted]

Podpis vedoucí(ho) práce | Podpis vedoucí(ho) ústavu/katedry | Podpis děkana(ky)

III. PŘEVZETÍ ZADÁNÍ

Diplomant bere na vědomí, že je povinen vypracovat diplomovou práci samostatně, bez cizí pomoci, s výjimkou poskytnutých konzultací. Seznam použité literatury, jiných pramenů a jmen konzultantů je třeba uvést v diplomové práci.

26. 7. 2017 Tomáš Pankrác

Datum převzetí zadání | Podpis studenta

Declaration

Prohlašuji, že jsem předloženou práci vypracoval samostatně a že jsem uvedl veškeré použité informační zdroje v souladu s Metodickým pokynem o dodržování etických principů při přípravě vysokoškolských závěrečných prací.

I declare that I finished this work personally and all sources used are provided.

V Taipei dne: 26.7.2017 Podpis autora práce: Tomáš Pakosć

Abstract

Novel design of compact integrated 8-Channel demultiplexer based on contra-directional Bragg assisted coupler for LAN-WDM is presented. Utilizing sub-wavelength waveguide for not only guiding the light, but also as reflecting Bragg structure allowing for easier parameter tuning, bigger sized structure resulting in better precision and fabrication error tolerance. Extensive overview of electromagnetic field theory is addressed, to provide background for analytic description and calculation of various parameters. Design parameters are also investigated by simulations in Lumerical Suite software and resulting spectral characteristics give flat top spectral responses with adjacent channel suppression better than 30 dB and insertion loss less than 1 dB.

Keywords: integrated, demultiplexer, contra-directional, coupler, silicon-on-insulator, Bragg grating, subwavelength waveguide, LAN-WDM

Abstrakt

V této práci je popsán návrh 8 kanálového demultiplexeru na principu kontra-direkcionální optické vazby s Braggovou mřížkou pro LAN-WDM vlnový multiplex. V návrhu je nově použit segmentovaný vlnovod, jak pro vedení světla, tak jako periodická struktura. V práci je poskytnut souhrn teorie elektromagnetického pole nezbytný pro analytický odhad a výpočet navrhované struktury. Parametry návrhu jsou zkoumané simulacemi v softwarové sadě Lumerical Suite. Výsledkem je kompletní návrh pro všechny kanály se spektrálními charakteristikami se vstupními ztrátami menšími než 1 dB a potlačením sousedních kanálů více než 30 dB.

Klíčová slova: integrovaný, demultiplexer, kontra-direkcionální, vazba, silicon-on-insulator, Braggova mřížka, segmentovaný vlnovod, LAN-WDM

Acknowledgments

I would like to express my deepest gratitude my advisors, prof. San-Liang Lee from National Taiwan University of Science and Technology and doc. Ing. Vítězslav Jeřábek, CSc., from Czech Technical University, for their guidance and help throughout my studies at home in Czech Republic as well as in Taiwan, giving me invaluable advice and means to continue developing my knowledge and skills. I would also like to thank all my friends, at home and in Taiwan, making my stay unforgettable. Last, but not least, I would like to thank my family, who supported me in my plan to move half the world away for more than a year in hopes of new international experiences.

Contents

List of Figures

List of Tables

Chapter 1

Introduction

1.1 Background

The need for speed and communication capacity is ever increasing and silicon-on-insulator passive devices can provide answer for many needs with great advantage of compatibility with classic CMOS fabrication technologies. One of the most currently used techniques for high speed communication over optical fiber is wavelength division multiplexing (WDM). WDM provides high bandwidth using data carriers of different wavelengths over one communication channel at the same time and therefore multiplying the data rate. Grating assisted contra directional couplers are well known structure for WDM demultiplexers. Used maily for CWDM [1], there is no design for LAN-WDM as of yet. Usual construction includes waveguide with corrugations on sidewalls or in the slab between them. These corrugations are of usually very small, posing challenge for fabrication methods. From the nature of the structure, we face many trials while designing, such as backreflections, crosstalk between channels and sensitivity to fabrication error.

1.2 Motivation

Current solutions for LAN-WDM multi/de-multiplexing are implemented as compact thin filter in a direct bounce "zig-zag" pattern. This solution has overall

very good properties, such as insertion loss less than 1.5dB and adjacent channel suppression more than 30dB, however high angular alignment of collimators and filters $\pm 0.03\,\mathrm{deg}$ is needed [2]. Utilizing free space propagation and classical optics with partially refractive mirrors and collimating lens makes it impractical other integrated parts of communication chain.

Therefore, novel integrated 8 channel de-multiplexer is proposed in this thesis. Based on contra-directional grating assisted couplers, this novel design involves subwavelength grating waveguide (SWG), effectively guiding light and acts as Bragg grating as well. The purpose of this work is to investigate this novel technique, provide theoretical explanation derived from elementary electromagnetic field theory, perform calculations using coupled mode theory and verify the idea by numerical simulation in Lumerical Suite. In the process, several design parameters will be considered and described to provide robust tool set for de-multiplexed channel wavelength design. In the end, we will be left with method how to precisely tune demultiplexer wavelength with variation of waveguides widths and subwavelength waveguides pitch and give numerical results corresponding to LAN-WDM channels. Resulting spectral characteristics show insertion loss of less than 1 dB and very high adjacent channel suppression of more than 30 dB.

1.3 Summary of content

In chapter two, we provide a brief introduction to the issues of optical telecommunication, multiplexing, overview of LAN-WDM standard and then continue with extensive theoretical derivation of electromagnetic wave and waveguide theory, in chapter three proposed design is introduced and calculated with analytical approach, next, in chapter four design parameters of proposed structure are investigated with bandstructure and spectral simulation. Finally, the conclusion with an overview of achieved results and proposal for future work is given.

Chapter 2

Theoretical Overview

2.1 Optical telecommunication

2.1.1 Multiplexing, Channel Link

Channel multiplexing over single fiber is a simple way to extend channel capacity with current infrastructure. Multiplexing can be realized through time domain, frequency domain, and recently investigated by mode separation. The methods are called time-division multiplexing (TDM), frequency division multiplexing (FDM) and mode-division multiplexing (MDM) respectively. Frequency-division multiplexing in optical systems is commonly referred to as wavelength-division multiplexing (WDM) for the optical domain nature of transmission signals.
The basic principle behind WDM is the transmission of multiple carriers of varying wavelengths over one optical fiber. Each carrier is modulated separately in the transmitter by either direct or indirect laser modulation.
Digital signal comprised of zeros and ones corresponding to on and off state can be easily achieved by modulating the current through laser diode. However, the maximum transmission frequency is limited by the frequency response of driving circuits and time constants of the laser diode. Furthermore, frequency chirp (output frequency shift with driving signal) is introduced into the output signal and extinction ratio is limited because laser diode current has to be kept above threshold current so it is never truly in the off state.

By modulating the laser output light directly, we can negate the diode transient problems in exchange for higher overall complexity. The laser is operating in continuous wave regime and the light propagates through material that can change its optical properties by applying an electric field. Either by changing absorption spectra so the material becomes opaque or altering a refractive index to change phase and consequently take advantage of constructive or destructive interference.

Next, all light signals are combined together in a multiplexer. On the receiver side, this signal is demultiplexed back into separate carriers. [3].

Wavelength bands useful for optical communications, so-called communication windows, are given by characteristics of the optical fiber. 2.1a shows attenuation and dispersion of traditional fiber and its relation with communication windows. For high-speed communications, the second and third window is used. At 1300 nm, the second window of 200 nm takes advantage of no dispersion at cost of higher attenuation around 0.5dB/km. At 1550 nm, the third window has similar size, but attenuation is the lowest. In modern fibers, the peak at 1400 nm, caused by hydroxyl ion OH^- impurities, is eliminated and the attenuation is due to Rayleigh diffraction [4]. Communication windows are split into several transmission bands, from original O-band to newest U/XL band [5]. C and L bands are used for high-speed, long distance communication for their low attenuation (¡0.2 dB/km)[5]. Communication bands schematic is shown in 2.1b Dense wavelength division multpiplexing (DWDM) and Erbium Doped Fiber amplifiers allow for unprecedented speeds and distances, but at relatively high cost. C and L band nowadays allow channel spacing as low as 12,5 GHz [6].

2.1.2 LAN-WDM Channel Design

Until recently, there were two main standards for wavelength division multiplexing; Coarse Wavelength Division Multiplex (CWDM) and Dense Wavelength Division Multiplex (DWDM).

CWDM is designed for use with cheap solutions e.g. omitting temperature control. CWDM is used for low speed and short optical communication networks.

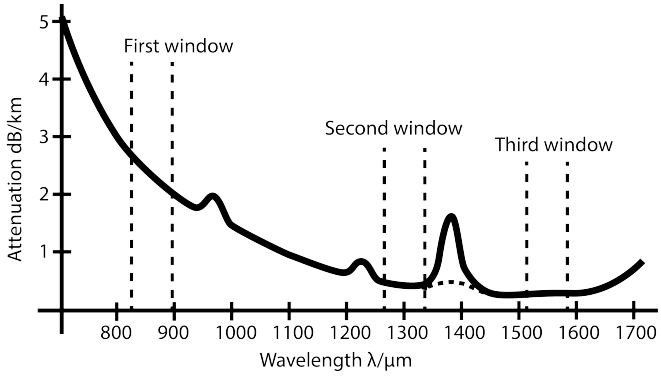

(a)

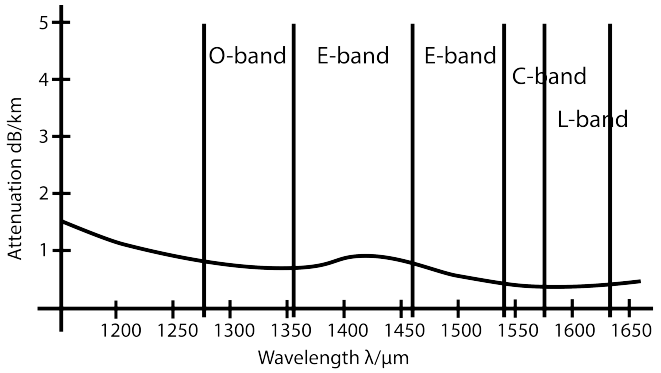

(b)

Figure 2.1: (a) schematic of telecommunication windows (b) telecommunication bands [7]

For longer and faster communication than 10km and 10Gbit/s, the cost of temperature control becomes negligible compared to total cost of Transmit Optical Sub-Assembly (TOSA). For 4x25G TOSA the TEC cost is only 1% to 4%. Each channel has to be relatively wide and widely spaced, ITU-T Recommendation G.694.2 specifies channel spacing of 20nm with expected channel width better than $\pm 6 - 7nm$ from center wavelength [8]. These properties limit the number of usable channels.

DWDM is meant for maximizing communication speed in exchange for higher cost and increased complexity. Channel spacing varies from 12.5GHz to 100GHz. The channel spacing has evolved from historical 100GHz by consecutive dividing by two up to 12.5GHz [6].

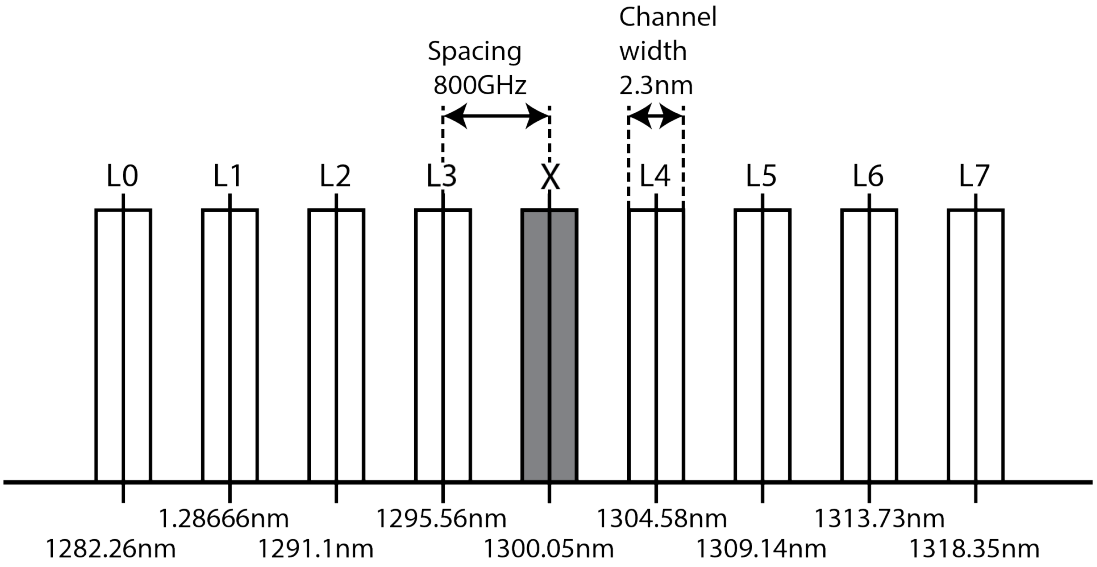

Figure 2.2: Grid of LAN-WDM for 8 channels L0 - L7, with one empty channel at 230.6THz (1300.05nm) to separate L0 - L3 and L4 - L7, channel spacing is 800GHz ($\approx 4.5nm$) and channel width is 400GHz ($\approx 2.3nm$)

Local Area Wavelength Division Multiplexing (LAN-WDM) is a compromise between both of these technologies. LAN-WDM channel grid is set in a wider spacing of channels 800GHz [9], which doesn't pose strict requirements at laser frequency stability as it is in DWDM. Our proposed LAN-WDM grid consists of 8 channels, L0 - L7, separated in two groups, L0 - L3 and L4 - L7, with one empty channel in between at 230.6 THz (1300.05 nm), viz. Figure 2.2, Tab. 2.1. For 25G and higher communication speeds, cooled lasers have a much higher yield as opposed to the uncooled version, which has problems with low output power due to high operating temperature. After all, this yield difference is much more important than added costs for cooling and packaging.

Chan.	L0	L1	L2	L3	X
$\lambda(\mu m)$	1.2822	1.2866	1.2911	1.2955	1.30005
$f(THz)$	233.8	233	232.3	231.4	230.6
Chan.	L4	L5	L6	L7	-
$\lambda(\mu m)$	1.3045	1.3091	1.3137	1.3183	-
$f(THz)$	229.8	229	228.2	227.4	-

Table 2.1: Proposed 8-Channel LAN-WDM grid L0 - L7 with empty channel at 230.6THz for separation of L0 - L3 and L4 - L7 into two groups

2.2 Waveguide Theory and Periodic structures

2.2.1 General formalism for non-stationary electromagnetic field

In this section, brief overview of fudnamental problems in electromagnetic theory is presented. Later in this work, this knowledge will be used for an analytical derivation of the proposed structure. Such derivations have been done in numerous literature, here mainly [10–12] are used as source of information.

Two fundamental relationships, often called Maxwell's equations, are given for electromagnetic field,

$$\nabla \times \boldsymbol{E} = -\frac{\partial \boldsymbol{B}}{\partial t} \tag{2.1}$$

$$\nabla \times \boldsymbol{H} = \boldsymbol{J} + \frac{\partial \boldsymbol{D}}{\partial t} \tag{2.2}$$

All components of electromagnetic field in these equations are vector functions, describing vectors in all points of space and time. We can rewrite them using scalar functions for each x, y and z component, giving us instantaneous value of vector in given space. For electric field written in Cartesian coordinate

system

$$\boldsymbol{E} = \boldsymbol{E}(x,y,z,t) = \mathbf{x_0} E_x(x,y,z,t) + \mathbf{y_0} E_y(x,y,z,t) + \mathbf{z_0} E_z(x,y,z,t) \tag{2.3}$$

and vector operator Nabla

$$\nabla = \left(\frac{\partial}{\partial x}, \frac{\partial}{\partial y}, \frac{\partial}{\partial z} \right) \tag{2.4}$$

Taking left side of Eq. (2.1) and rewriting we get

$$\nabla \times \boldsymbol{E} = \nabla \times \boldsymbol{E}(x,y,z,t) = \begin{vmatrix} \mathbf{x_0} & \mathbf{y_0} & \mathbf{z_0} \\ \frac{\partial}{\partial x} & \frac{\partial}{\partial y} & \frac{\partial}{\partial z} \\ E_x(x,y,z,t) & E_y(x,y,z,t) & E_z(x,y,z,t) \end{vmatrix} =$$
$$\mathbf{x_0} \left(\frac{\partial E_z(x,y,z,t)}{\partial y} - \frac{\partial E_y(x,y,z,t)}{\partial z} \right) +$$
$$\mathbf{y_0} \left(\frac{\partial E_x(x,y,z,t)}{\partial z} - \frac{\partial E_z(x,y,z,t)}{\partial x} \right) +$$
$$\mathbf{z_0} \left(\frac{\partial E_y(x,y,z,t)}{\partial x} - \frac{\partial E_x(x,y,z,t)}{\partial y} \right) \tag{2.5}$$

and right side of Eq. (2.1) can be rewritten

$$\frac{\partial \boldsymbol{B}}{\partial t} = \frac{\partial}{\partial t} \boldsymbol{B}(x,y,z,t) = \mathbf{x_0} \frac{\partial}{\partial t} B_x(x,y,z,t) +$$
$$\mathbf{y_0} \frac{\partial}{\partial t} B_x(x,y,z,t) + \mathbf{z_0} \frac{\partial}{\partial t} B_x(x,y,z,t) \tag{2.6}$$

Electromagnetic field components are bound by to each other by

$$\boldsymbol{D} = \varepsilon \boldsymbol{E} \tag{2.7}$$

$$\boldsymbol{J} = \sigma \boldsymbol{E} \tag{2.8}$$

$$\boldsymbol{B} = \mu \boldsymbol{H} \tag{2.9}$$

where D is electric displacement, E is electric field, J is current density, B is magnetic field, H is called magnetic field strength. With assumption of homogeneous, isotropic, non-conductive (lossless), dielectric (non-magnetic) medium, then

$$\boldsymbol{D} = \varepsilon_0 \varepsilon_r \boldsymbol{E} \tag{2.10}$$

where ε_0 is permittivity of vacuum

$$\varepsilon_0 \approx \frac{1}{36\pi} \cdot 10^{-9} \tag{2.11}$$

and ε_r is relative permittivity of the medium, in optics often written as index of refraction

$$n = \sqrt{\varepsilon_r} \tag{2.12}$$

which is a ratio of phase speed of light in dielectric material vs vacuum. Next

$$\boldsymbol{B} = \mu_0 \boldsymbol{H}[T] \tag{2.13}$$

where μ_0 is permeability of vacuum

$$\mu_0 = 4\pi \cdot 10^{-7} \tag{2.14}$$

and due to electrically non-conductive material we have

$$\sigma = 0, \boldsymbol{J} = \sigma \boldsymbol{E} = 0 \tag{2.15}$$

Permittivity and permeability are bound together by mutual equation with speed of light

$$c = \frac{1}{\sqrt{\mu_0 \varepsilon_0}} \approx 3 \cdot 10^8 [m/s] \tag{2.16}$$

Equations (2.1) and (2.2) can be rewritten using only $\boldsymbol{E}$ and $\boldsymbol{H}$

$$\nabla \times \boldsymbol{E} = -\mu_0 \frac{\partial \boldsymbol{H}}{\partial t} \nabla \times \boldsymbol{H} = \varepsilon_0 \varepsilon_r \frac{\partial \boldsymbol{E}}{\partial t} \tag{2.17}$$

which can be solved using another "Nabla" operator

$$\nabla \times (\nabla \times \boldsymbol{E}) = -\mu_0 \frac{\partial}{\partial t} \nabla \times \boldsymbol{H} \tag{2.18}$$

and equivalently vector identity

$$\nabla \times (\nabla \times \boldsymbol{E}) = \nabla (\nabla \cdot \boldsymbol{E}) - \nabla^2 \boldsymbol{E} \tag{2.19}$$

In case we ignore all sources, we can set the following

$$\nabla (\nabla \cdot \boldsymbol{E}) = 0 \tag{2.20}$$

and final formula in partial derivative form for $\boldsymbol{E}$ is

$$\nabla^2 \boldsymbol{E} - \mu_0 \varepsilon_0 \varepsilon_r \frac{\partial^2 \boldsymbol{E}}{\partial t^2} = 0 \tag{2.21}$$

The final differential equation for $\mathbf{E}$

$$\begin{aligned}
&\nabla^2 \boldsymbol{E}(x,y,z,t) = \\
&\mathbf{x_0}\left(\frac{\partial^2 \boldsymbol{E}_{\mathrm{x}}(x,y,z,t)}{\partial x^2} + \frac{\partial^2 \boldsymbol{E}_{\mathrm{x}}(x,y,z,t)}{\partial y^2} + \frac{\partial^2 \boldsymbol{E}_{\mathrm{x}}(x,y,z,t)}{\partial z^2}\right) + \\
&\mathbf{y_0}\left(\frac{\partial^2 \boldsymbol{E}_{\mathrm{y}}(x,y,z,t)}{\partial x^2} + \frac{\partial^2 \boldsymbol{E}_{\mathrm{y}}(x,y,z,t)}{\partial y^2} + \frac{\partial^2 \boldsymbol{E}_{\mathrm{y}}(x,y,z,t)}{\partial z^2}\right) + \\
&\qquad \mathbf{z_0}\left(\frac{\partial^2 \boldsymbol{E}_{\mathrm{z}}(x,y,z,t)}{\partial x^2} + \frac{\partial^2 \boldsymbol{E}_{\mathrm{z}}(x,y,z,t)}{\partial y^2} + \frac{\partial^2 \boldsymbol{E}_{\mathrm{z}}(x,y,z,t)}{\partial z^2}\right)
\end{aligned} \tag{2.22}$$

assuming only harmonic signals in time domain then for each spacial component applies

$$E_x(x,y,z,t) = E_{mx}(x,y,z)\ \sin(\omega t + \varphi_{x(x,y,z)}) \tag{2.23}$$

$$E_y(x,y,z,t) = E_{my}(x,y,z)\ \sin(\omega t + \varphi_{y(x,y,z)}) \tag{2.24}$$

$$E_z(x,y,z,t) = E_{mz}(x,y,z)\ \sin(\omega t + \varphi_{z(x,y,z)}) \tag{2.25}$$

where E_{mi} is amplitude of each component and φ_i is phase shift. Equations are possible to further simplify using phasors

$$E_i(x,y,z) = E_{mi} e^{j\varphi_{i(x,y,z)}} \tag{2.26}$$

and the vector functions becomes

$$\mathbf{E}(x,y,z) = \mathbf{x_0} E_x(x,y,z) + \mathbf{y_0} E_y(x,y,z) + \mathbf{z_0} E_z(x,y,z) \tag{2.27}$$

and the relationship between phasors and time domain function

$$E_x(x,y,z,t) = \mathrm{Im}\left(E_{mx}(x,y,z)\ \mathrm{e}^{j\omega t}\right) \tag{2.28}$$

$$E_y(x,y,z,t) = \mathrm{Im}\left(E_{my}(x,y,z)\ \mathrm{e}^{j\omega t}\right) \tag{2.29}$$

$$E_z(x,y,z,t) = \mathrm{Im}\left(E_{mz}(x,y,z)\ \mathrm{e}^{j\omega t}\right) \tag{2.30}$$

Using phasors and solving the second time derivative the Equation (2.21) will be

$$\nabla^2 \mathbf{E} + \omega^2 \mu_0 \varepsilon_0 \varepsilon_r \mathbf{E} = 0 \tag{2.31}$$

then we define constant, called propagation constant

$$k = \omega\sqrt{\mu_0\varepsilon_0\varepsilon_r} = \frac{\omega}{c}\sqrt{\varepsilon_r} \tag{2.32}$$

and Equation (2.31) can be rewritten

$$\nabla^2\mathbf{E}+k^2\mathbf{E} = 0 \tag{2.33}$$

This is so called homogeneous Helmholtz equation and rewritten for each spatial component looks like

$$\begin{aligned}
\nabla^2\mathbf{E}+k^2\mathbf{E} = \\
&= \mathbf{x_0}\left(\frac{\partial^2 E_{\mathrm{x}}(x,y,z)}{\partial x^2} + \frac{\partial^2 E_{\mathrm{x}}(x,y,z)}{\partial y^2} + \frac{\partial^2 E_{\mathrm{x}}(x,y,z)}{\partial z^2}\right) + \\
&+ \mathbf{y_0}\left(\frac{\partial^2 E_{\mathrm{y}}(x,y,z)}{\partial x^2} + \frac{\partial^2 E_{\mathrm{y}}(x,y,z)}{\partial y^2} + \frac{\partial^2 E_{\mathrm{y}}(x,y,z)}{\partial z^2}\right) + \\
&+ \mathbf{z_0}\left(\frac{\partial^2 E_{\mathrm{z}}(x,y,z)}{\partial x^2} + \frac{\partial^2 E_{\mathrm{z}}(x,y,z)}{\partial y^2} + \frac{\partial^2 E_{\mathrm{z}}(x,y,z)}{\partial z^2}\right) + \\
&+ k^2\left(\mathbf{x_0}E_x(x,y,z) + \mathbf{y_0}E_y(x,y,z) + \mathbf{z_0}E_z(x,y,z)\right) = 0
\end{aligned} \tag{2.34}$$

2.2.2 Solution to Helmholtz equation for electromagnetic plane wave

Harmonic electromagnetic plane wave is the simplest solution for this equation. With assumption that electric field has only x component which is changing only in z direction, then

$$E_x, E_y = 0, E_z = 0 \tag{2.35}$$

$$E_x = f(z), \quad E_x \neq f(x,y) \tag{2.36}$$

and Equation (2.33) is simplified into

$$\frac{d^2 E_{\mathrm{x}}(z)}{dz^2} + k^2 E_{\mathrm{x}}(z) = 0 \tag{2.37}$$

representing plane wave propagating in z direction. Solution to this equation is phasor of electric field

$$E_{\mathrm{x}}(z) = E_0 e^{-j\,k\,z} \tag{2.38}$$

where

$$E_0 = E_m e^{j\,\varphi_0} \tag{2.39}$$

is magnitude of phasor on $z = 0$. Transforming the phasor to time domain, we get

$$E_{\mathrm{x}}(z,t) = E_{\mathrm{m}} \sin(\omega t - k\,z + \varphi_0) \tag{2.40}$$

Phasor of intensity of magnetic field is derived back from Equation (2.17) by substitution for electric field

$$H_y(z) = \frac{E_{\mathrm{x}}(z)}{Z} = \frac{E_0}{Z} e^{-j\,k\,z} = H_0 e^{-j\,k\,z} \tag{2.41}$$

Intensity of magnetic field will only have component in y direction. Phasors of electric and magnetic field are bound by so called characteristic impedance of unbounded space

$$Z = \frac{\omega\mu_0}{k} = \frac{1}{\sqrt{\varepsilon_r}} \sqrt{\frac{\mu_0}{\varepsilon_0}} \approx \frac{120\pi}{\sqrt{\varepsilon_r}} \tag{2.42}$$

2.2.3 Solution of Helmholtz equation pro electromagnetic wave propagating in general direction

Equation (2.34) can be separated into three identical equations, one for each individual components $i = x, y, z$

$$\frac{\partial^2 E_i(x,y,z)}{\partial x^2} + \frac{\partial^2 E_i(x,y,z)}{\partial y^2} + \frac{\partial^2 E_i(x,y,z)}{\partial z^2} + k^2 E_i(x,y,z) = 0 \tag{2.43}$$

Under assumption, that we can get solution of this equation in form of multiplication of these three functions for x, y, z

$$E_i(x,y,z) = X(x)Y(y)Z(z) \tag{2.44}$$

Plugging expected solution (2.44) back into (2.43), we can get following differential equations

$$\frac{1}{\mathrm{X}(x)} \frac{\partial^2 \mathrm{X}(x)}{\partial x^2} + \frac{1}{\mathrm{Y}(y)} \frac{\partial^2 \mathrm{Y}(y)}{\partial y^2} + \frac{1}{\mathrm{Z}(z)} \frac{\partial^2 \mathrm{Z}(z)}{\partial z^2} + \mathrm{k}^2 = 0 \tag{2.45}$$

where each part represents partial equation whose right side has to remain zero. We can write thee equations using so called separation coefficient this form

$$\frac{1}{\mathrm{X}(x)}\frac{\partial^2 \mathrm{X}(x)}{\partial x^2} = -\mathrm{k_x}^2 \tag{2.46}$$

$$\frac{1}{\mathrm{Y}(y)}\frac{\partial^2 \mathrm{Y}(y)}{\partial y^2} = -\mathrm{k_y}^2 \tag{2.47}$$

$$\frac{1}{\mathrm{Z}(z)}\frac{\partial^2 \mathrm{Z}(z)}{\partial z^2} = -\mathrm{k_z}^2 \tag{2.48}$$

To ensure equality and zero of the Equation (2.45), each coefficient has to be

$$\mathrm{k}^2 = \mathrm{k_x}^2 + \mathrm{k_y}^2 + \mathrm{k_z}^2 \tag{2.49}$$

After solving each partial equation from (2.46), we get the sought functions

$$\mathrm{X}(x) = \mathrm{C}_1 e^{-j\mathrm{k_x}\cdot x} + \mathrm{C}_2 e^{+j\mathrm{k_x}\cdot x} \tag{2.50}$$

$$\mathrm{Y}(y) = \mathrm{C}_3 e^{-j\mathrm{k_y}\cdot y} + \mathrm{C}_4 e^{+j\mathrm{k_z}\cdot z} \tag{2.51}$$

$$\mathrm{Z}(z) = \mathrm{C}_5 e^{-j\mathrm{k_z}\cdot z} + \mathrm{C}_6 e^{+j\mathrm{k_z}\cdot z} \tag{2.52}$$

and the final solution for phasors of each component is

$$\begin{aligned}&\mathrm{E_i}(x,y,z) = \mathrm{X}(x)\mathrm{Y}(y)\mathrm{Z}(z) = \\ &\left(\mathrm{C}_1 e^{-j\mathrm{k_x}\cdot x} + \mathrm{C}_2 e^{+j\mathrm{k_x}\cdot x}\right)\left(\mathrm{C}_3 e^{-j\mathrm{k_y}\cdot y} + \mathrm{C}_4 e^{+j\mathrm{k_y}\cdot y}\right)\left(\mathrm{C}_5 e^{-j\mathrm{k_z}\cdot z} + \mathrm{C}_6 e^{+j\mathrm{k_z}\cdot z}\right)\end{aligned} \tag{2.53}$$

and assuming only forward propagating wave without reflections

$$\mathrm{E_i}(x,y,z) = \mathrm{C}_1\mathrm{C}_3\mathrm{C}_5 e^{-j\mathrm{k_x}\cdot x} e^{-j\mathrm{k_y}\cdot y} e^{-j\mathrm{k_z}\cdot z} = \mathrm{E_{i0}} e^{-j(\mathrm{k_x}\cdot x + \mathrm{k_y}\cdot y + \mathrm{k_z}\cdot z)} = \mathrm{E_{i0}} e^{-j\mathbf{k}\cdot\mathbf{r}} \tag{2.54}$$

where E_{i0} is phasor at the origin of coordinates. The exponent can also be written as a dot product of vectors $\mathbf{k}$ and $\mathbf{r}$, where $\mathbf{k}$ is so called wave vector, showing direction of propagation of electromagnetic wave, perpendicular to wave plane and its absolute value is equal to propagation constant (2.32). Its components can be understood as projection of $\mathbf{k}$ onto the axes, because then Equation (2.49) will hold true

$$\mathbf{k} = (k_x, k_y, k_z) \tag{2.55}$$

r is so called position vector or radius vector and it specifies spatial position of the field calculation

$$\mathbf{r} = (x, y, z) \tag{2.56}$$

Resulting equation for phasor of intensity of electric field can be written as

$$\mathbf{E}(x, y, z) = (\mathbf{x_0}\mathrm{E_{x0}} + \mathbf{y_0}\mathrm{E_{y0}} + \mathbf{z_0}\mathrm{E_{z0}})\, e^{-j\mathbf{k}\cdot\mathbf{r}} = \mathbf{E_0} e^{-j\mathbf{k}\cdot\mathbf{r}} \tag{2.57}$$

2.2.4 Electromagnetic wave incident on material interface - reflection, refraction and evanescent wave

Electromagnetic wave incident on interface of dielectric materials at angle θ_i behaves according to Snell's laws

$$\theta_R = \theta_i \tag{2.58}$$

$$k_1 \sin(\theta_i) = k_2 \sin(\theta_T) \tag{2.59}$$

It can be rewritten using permittivity

$$\sqrt{\varepsilon_{\mathrm{r1}}}\sin(\vartheta_{\mathrm{i}}) = \sqrt{\varepsilon_{\mathrm{r2}}}\sin(\vartheta_{\mathrm{T}}) \tag{2.60}$$

For angle of refraction then

$$\vartheta_T = \arcsin\left(\sqrt{\frac{\varepsilon_{r1}}{\varepsilon_{r2}}} sin(\vartheta_i)\right) \tag{2.61}$$

Magnitude of phasor of reflected and transmitted wave in relation to the incident wave is given by coefficient of reflection and transmission respectively

$$\mathrm{R} = \frac{\mathrm{E_{R0}}}{\mathrm{E_{i0}}} \tag{2.62}$$

$$\mathrm{T} = \frac{\mathrm{E_{T0}}}{\mathrm{E_{i0}}} \tag{2.63}$$

Magnitude of reflection coefficient is dependent on the polarization of electromagnetic wave, which corresponds to orientation of vector of electric field to the normal of the interface. We recognize two types of polarization, horizontal and normal. Horizontal polarization has vector of electric field perpendicular to the plane of incidence and in normal polarization, orientation of electric field is parallel to the plane of incidence. Naturally, light doesn't have to adhere to these

two situations and the electric field can be oriented in any direction. Reflection and transmission coefficients for each polarization are defined as

$$\mathrm{R}_{\parallel} = \frac{\sqrt{\varepsilon_{r1}}\cos(\vartheta_T) - \sqrt{\varepsilon_{r2}}\cos(\vartheta_i)}{\sqrt{\varepsilon_{r1}}\cos(\vartheta_T) + \sqrt{\varepsilon_{r2}}\cos(\vartheta_i)} \quad \mathrm{R}_{\perp} = \frac{\sqrt{\varepsilon_{r1}}\cos(\vartheta_i) - \sqrt{\varepsilon_{r2}}\cos(\vartheta_T)}{\sqrt{\varepsilon_{r1}}\cos(\vartheta_i) + \sqrt{\varepsilon_{r2}}\cos(\vartheta_T)} \tag{2.64}$$

$$T_{\parallel} = \frac{2\sqrt{\varepsilon_{r1}}\cos(\vartheta_T)}{\sqrt{\varepsilon_{r1}}\cos(\vartheta_T) + \sqrt{\varepsilon_{r2}}\cos(\vartheta_i)} \quad T_{\perp} = \frac{2\sqrt{\varepsilon_{r1}}\cos(\vartheta_i)}{\sqrt{\varepsilon_{r1}}\cos(\vartheta_i) + \sqrt{\varepsilon_{r2}}\cos(\vartheta_T)} \tag{2.65}$$

If incident wave transmits into medium with higher permittivity $\varepsilon_{r1} < \varepsilon_{r2}$ then

$$\sqrt{\frac{\varepsilon_{r1}}{\varepsilon_{r2}}} sin(\vartheta_i) < 1 \tag{2.66}$$

and angle of refraction is then smaller than angle of incidence $\vartheta_T < \vartheta_i$ and the light is bent "towards normal", viz. Figure 2.3. In the other case, where wave is

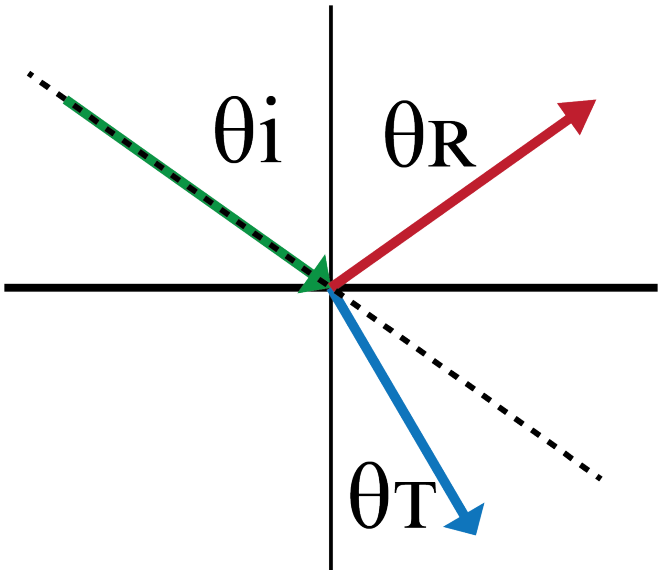

Figure 2.3: Reflection and transmission towards normal

propagating into material with higher permittivity,$\varepsilon_{r1} > \varepsilon_{r2}$, then from (2.62)

$$\vartheta_T > \vartheta_i \tag{2.67}$$

and light bends "from normal", viz. Figure 2.4. At one specific angle of incidence, called critical angle

$$\vartheta_i = \vartheta_{cr} = \arcsin\sqrt{\frac{\varepsilon_{r2}}{\varepsilon_{r1}}} \tag{2.68}$$

the angle is $\vartheta_T = \frac{\pi}{2}$, viz. Figure 2.5 From this angle, there is so called total

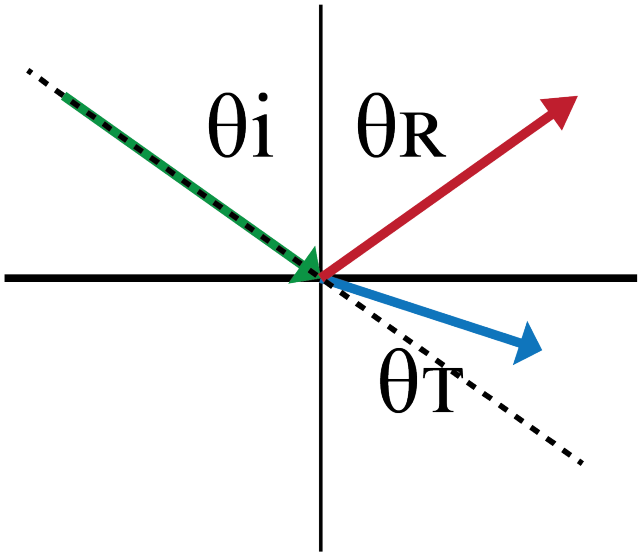

Figure 2.4: Reflection and transmission from normal

reflection effect, after plugging $\cos(\vartheta_T) = \cos(\frac{\pi}{2}) = 0$ to (2.64), we get

$$\mathrm{R}_{\parallel} = -1$$

$$\mathrm{R}_{\perp} = 1$$

Therefore, for angle bigger than critical, argument of complex reflection coefficient changes, but its magnitude stays the same, equal to 1. Reflected and transmitted waves are changing their mutual phase, but the reflection is still complete

$$\vartheta_i \geqslant \vartheta_{cr} \qquad \left|\mathrm{R}_{\parallel}\right| = \left|\mathrm{R}_{\perp}\right| = 1 \tag{2.69}$$

In area under interface, so called evanescent wave will be propagating and its properties can be assessed by plugging transmission angle into Equation (2.54)

$$E_T(x, y, z) = \mathrm{E}_{T0} e^{-j\mathrm{k}_2(\sin(\vartheta_T)\cdot x + \cos(\vartheta_T)\cdot z)} \tag{2.70}$$

For incident angle $0 < \vartheta_i < pi/2$ is

$$sin(\vartheta_T) = \sqrt{\frac{\varepsilon_{r1}}{\varepsilon_{r2}}} sin(\vartheta_i) = p \tag{2.71}$$

real number and $\cos(\vartheta_T)$ is for $\varepsilon_{r1} > \varepsilon_{r2}$ and $\vartheta_i \geqslant \vartheta_{cr}$ purely imaginary

$$\cos(\vartheta_T) = \sqrt{1 - \sin^2(\vartheta_T)} = \sqrt{1 - \frac{\varepsilon_{r1}}{\varepsilon_{r2}} sin^2(\vartheta_i)} = \pm j\sqrt{\frac{\varepsilon_{r1}}{\varepsilon_{r2}} sin^2(\vartheta_i) - 1} = \pm jq \tag{2.72}$$

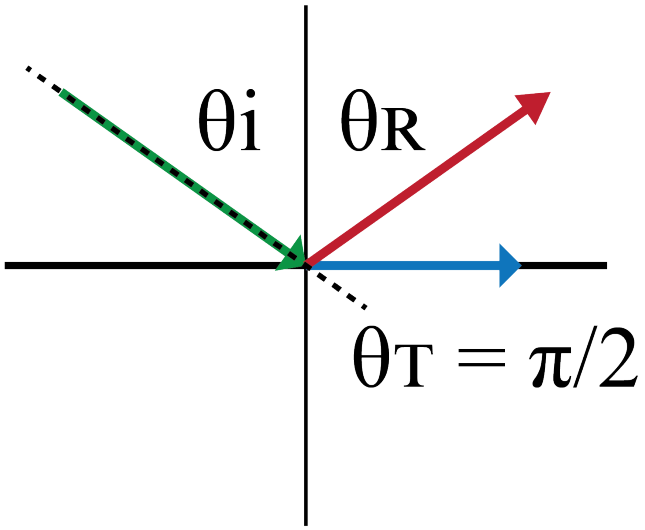

Figure 2.5: Critical angle of reflection

Solving the equation, we will find out, that amplitude is declining perpendicular to the interface with coefficient k_2q, and phase is changing along the interface x with k_2p. Such wave is called non-uniform.

$$E_T(x,y,z) = \mathrm{E}_{T0}e^{-jk_2(p\cdot x - jq\cdot z)} = \mathrm{E}_{T0}e^{-k_2q\cdot z}e^{-jk_2p\cdot x} \tag{2.73}$$

2.2.5 Guided wave

When electromagnetic wave is propagated along a structure with constant transverse dimensions x and y, formation of field with standing waves in transverse direction and traveling wave along z direction can be expected. From Helmholtz equation (2.34) we can then seek solution to partial functions (2.50) as

$$\mathrm{X}(x) = \mathrm{C}_1\cos(\mathrm{k_x}\cdot x) + \mathrm{C}_2\sin(\mathrm{k_x}\cdot x) \tag{2.74}$$

$$\mathrm{Y}(x) = \mathrm{C}_3\cos(\mathrm{k}_y\cdot y) + \mathrm{C}_4\sin(\mathrm{k}_y\cdot y) \tag{2.75}$$

$$\mathrm{Z}(z) = \mathrm{C}_5e^{-j\mathrm{k_z}\cdot z} \tag{2.76}$$

Yet unknown coefficient $\mathrm{k_x}$,k_y characterize shape of the standing wave in transverse direction, coefficient k_z is phase constant of guided wave along z direction. For these constants, separation equation has to hold

$$\mathrm{k}^2 = \mathrm{k_x}^2 + \mathrm{k_y}^2 + \mathrm{k_z}^2 \tag{2.77}$$

where k is unbound space propagation constant as in (2.32). General solution for each spatial component $i = x, y, z$ of electromagnetic field will be similar to (2.53)

$$\begin{aligned}&\mathrm{E_i}(x,y,z) = \mathrm{X}(x)\mathrm{Y}(y)\mathrm{Z}(z) = \\ &= \left(\mathrm{C}_1 \cos(\mathrm{k_x}\cdot x) + \mathrm{C}_2 \sin(\mathrm{k_x}\cdot x)\right)\left(\mathrm{C}_3 \cos(\mathrm{k}_y\cdot x) + \mathrm{C}_4 \sin(\mathrm{k}_y\cdot x)\right)\mathrm{C}_5 e^{-j\mathrm{k_z}\cdot z}\end{aligned} \tag{2.78}$$

General mutual relationship between electric and magnetic fields (2.5) can be rewritten with derivative along z direction $z : -jk_z$ into

$$\nabla \times \mathbf{E} = \nabla \times \mathbf{E}(x,y,z) = \begin{vmatrix} \mathbf{x_0} & y_\mathbf{0} & z_\mathbf{0} \\ \frac{\partial}{\partial x} & \frac{\partial}{\partial y} & -j\ k_z \\ E_x(x,y,z) & E_y(x,y,z) & E_z(x,y,z) \end{vmatrix} = -j\omega\mu_0 \mathbf{H} \tag{2.79}$$

and for each spatial component

$$\begin{aligned}\mathbf{x_0}\left(\frac{\partial E_z(x,y,z)}{\partial y} + j\ k_z E_y(x,y,z)\right) + y_\mathbf{0}\left(-jk_z E_x(x,y,z) - \frac{\partial E_z(x,y,z)}{\partial x}\right) + \\ + z_\mathbf{0}\left(\frac{\partial E_y(x,y,z)}{\partial x} - \frac{\partial E_x(x,y,z)}{\partial y}\right) = \\ - j\omega\mu_0\left(\mathbf{x_0} H_x(x,y,z) + y_\mathbf{0} H_y(x,y,z) + z_\mathbf{0} H_z(x,y,z)\right)\end{aligned} \tag{2.80}$$

2.2.6 Wave guided between dielectric layers

Assuming formation of TE modes, then electric field intensity has component only y direction and the other is zero. Considering the

$$E_y(x,z)$$

$$E_x = E_z = 0$$

using (2.80) we will find out, that intensity of magnetic field has to have these components

$$H_x(x,z) = -\frac{k_z}{\omega\mu_0} E_y(x,z) \tag{2.81}$$

$$H_z(x,z) = \frac{j}{\omega\mu_0}\frac{\partial E_y(x,z)}{\partial x} \tag{2.82}$$

Final solution of all coefficients can be found by writing general equations for each component and setting their mutual conditions. From (2.78) we can write basic relationship for y component of electric field intensity in the central, guiding layer. All constants C_i are joined together into constant E_{mx1} and ϕ

$$\mathrm{E_{y1}}(x,y,z) = \mathrm{C_5}\left(\mathrm{C_1}\cos(\mathrm{k_x}\cdot x) + \mathrm{C_2}\sin(\mathrm{k_x}\cdot x)\right)e^{-j\mathrm{k_z}\cdot z} = E_{mx1}\cos(\mathrm{k_x}\cdot x+\phi)e^{-j\mathrm{k_z}\cdot z} \tag{2.83}$$

Analogically, for components of magnetic fields

$$H_{x1}(x,z) = -\frac{k_z}{\omega\mu_0}E_y(x,z) = -\frac{k_z}{\omega\mu_0}E_{my1}\cos(\mathrm{k_{x1}}\cdot x+\phi)e^{-k_z z} \tag{2.84}$$

$$H_{z1}(x,z) = \frac{j}{\omega\mu_0}\frac{\partial E_{y1}(x,z)}{\partial x} = -\frac{j\mathrm{k_{x1}}}{\omega\mu_0}E_{my1}\sin(\mathrm{k_{x1}}\cdot x+\phi)e^{-k_z z} \tag{2.85}$$

In outer layers labeled as 2, electromagnetic wave will have evanescent wave form as in (2.73), where k_{x2} is the attenuation constant in transverse direction x, phase constant in z direction is the same as the guiding layer 1

$$E_{y2}(x,z) = E_{my2}e^{-k_{x2}\cdot x}\ e^{-jk_z z} \tag{2.86}$$

Each component of magnetic field in layer 2 will according to (2.81), (2.82) be

$$H_{x2}(x,z) = -\frac{k_z}{\omega\mu_0}E_{y2}(x,z) = -\frac{k_z}{\omega\mu_0}E_{my2}e^{-k_{x2}\cdot x}\ e^{-jk_z z} \tag{2.87}$$

$$H_{z2}(x,z) = \frac{j}{\omega\mu_0}\frac{\partial E_{y2}(x,z)}{\partial x} = -\frac{j\mathrm{k_{x2}}}{\omega\mu_0}E_{my2}e^{-k_{x2}\cdot x}\ e^{-jk_z z} \tag{2.88}$$

Boundary conditions on the interface of layers 1 and 2 arise from continuity of electromagnetic fields. Tangent component of intensity of electric and magnetic field at the boundary has to be the same from each side. For magnetic field and lower boundary $x = a$

$$H_{z1}(x=a,z) = H_{z2}(x=a,z) \tag{2.89}$$

From (2.85) and (2.88) we then get

$$\mathrm{k_{x1}}E_{my1}\sin(\mathrm{k_{x1}}\cdot\frac{h}{2}+\phi) = \mathrm{k_{x2}}E_{my2}e^{-k_{x2}\cdot\frac{h}{2}} \tag{2.90}$$

For electric field at the same boundary $x = a = h/2$

$$E_{y1}(x=\frac{h}{2},z) = E_{y2}(x=\frac{h}{2},z) \tag{2.91}$$

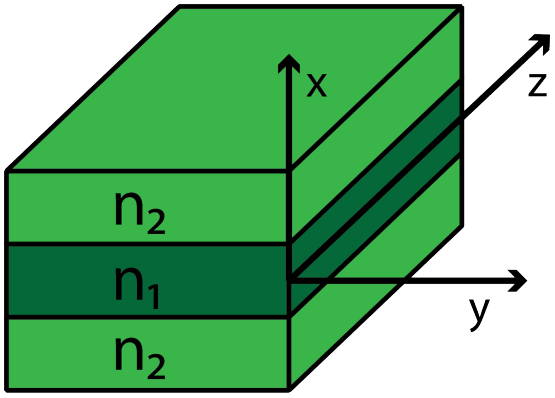

Figure 2.6: Illustration of slab waveguide

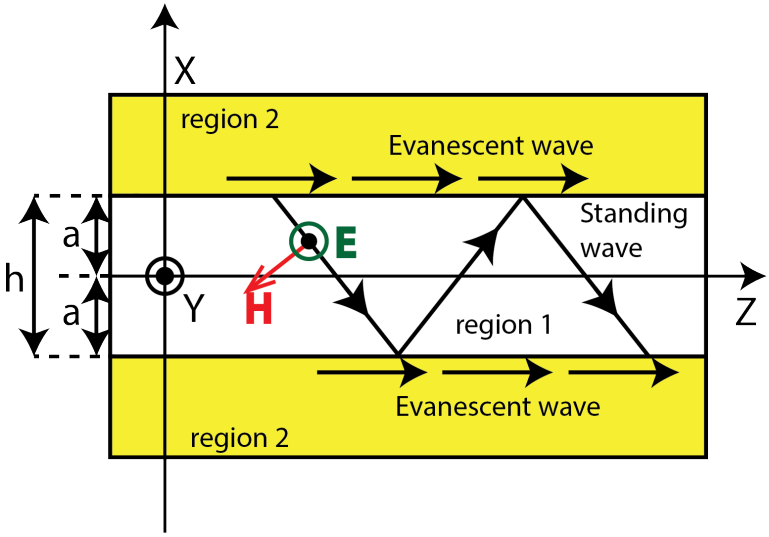

Figure 2.7: Cross section of slab waveguide structure with propagating TE mode

From (2.83) and (2.86) for this condition we have

$$E_{my1}\cos(\mathrm{k_x}\cdot\frac{h}{2}+\phi)=E_{my2}e^{-k_{x2}\cdot\frac{h}{2}} \tag{2.92}$$

By dividing equations (2.90) and (2.92) we get

$$\tan(\mathrm{k_{x1}}\cdot\frac{h}{2}+\phi)=\frac{\mathrm{k_{x2}}}{\mathrm{k_{x1}}} \tag{2.93}$$

and very similarly for $x=-h/2$

$$-\tan(-\mathrm{k_{x1}}\cdot\frac{h}{2}+\phi)=\frac{\mathrm{k_{x2}}}{\mathrm{k_{x1}}} \tag{2.94}$$

Subtracting Equations (2.93) and (2.94) we can eliminate parameter ϕ and we get so called dispersion equation, which gives us relationship between coefficients

in transverse direction

$$\mathrm{k_{x1}} \cdot h = 2 \tan^{-1}\left(\frac{\mathrm{k_{x2}}}{\mathrm{k_{x1}}}\right) + m \cdot \pi \tag{2.95}$$

where $m \cdot \pi$ represents period of function $\tan(-1)$ and it is mode number as well.

2.2.7 Generalized parameters

According to (2.77) following must hold true

$$\mathrm{k_{x1}} = \sqrt{\mathrm{k_1}^2 - \mathrm{k_z}^2} \quad , \qquad \mathrm{k}_{x2} = \sqrt{\mathrm{k_z}^2 - \mathrm{k_2}^2} \tag{2.96}$$

k_1, k_2 are propagation constants of plane wave of the same frequency in free space with same parameters, as in (2.32)

$$\mathrm{k_1} = \frac{\omega}{c}\sqrt{\varepsilon_{r1}} \quad , \qquad \mathrm{k_2} = \frac{\omega}{c}\sqrt{\varepsilon_{r2}} \tag{2.97}$$

From (2.96) then

$$\mathrm{k_{x1}} \cdot h = h\sqrt{k_1{}^2 - k_z{}^2} \quad , \qquad \mathrm{k_{x2}} \cdot h = h\sqrt{\mathrm{k_z}^2 - \mathrm{k_2}^2} \tag{2.98}$$

By adding both equations (2.98), we can eliminate longitudinal constant k_z and we define new parameter V, which frequency, layer parameters and dimension h dependent, called generalized frequency

$$\mathrm{h}\sqrt{\mathrm{k_{x1}}^2 + \mathrm{k_{x2}}^2} = h\sqrt{\mathrm{k_1}^2 + \mathrm{k_2}^2} = h\frac{\omega}{c}\sqrt{\varepsilon_{r1} - \varepsilon_{r2}} = V \tag{2.99}$$

dividing Equation (2.99) by V we can rewrite it

$$\sqrt{\left(\frac{\mathrm{h\ k_{x1}}}{V}\right)^2 + \left(\frac{\mathrm{h\ k_{x2}}}{V}\right)^2} = 1 \tag{2.100}$$

Then we can define new parameter b called generalized guide index

$$\left(\frac{\mathrm{k_{x2}} \cdot h}{V}\right)^2 = b = \frac{h^2\left(\mathrm{k_z}^2 - \mathrm{k_2}^2\right)}{V^2} = \frac{h^2\left(\frac{\omega}{c}\sqrt{\varepsilon_{r2}}\right) - \left(\frac{\omega}{c}\sqrt{N}\right)^2}{\left(h\frac{\omega}{c}\sqrt{\varepsilon_{r1} - \varepsilon_{r2}}\right)^2} = \frac{\varepsilon_{r2} - N}{\varepsilon_{r1} - \varepsilon_{r2}} \tag{2.101}$$

where N is equivalent permittivity and it is equal to magnitude of k_z of plane wave in unbound space.

Using these new parameters, we can rewrite first part of (2.100) as

$$\left(\frac{\mathrm{k_{x1}} \cdot h}{V}\right)^2 = 1 - b \tag{2.102}$$

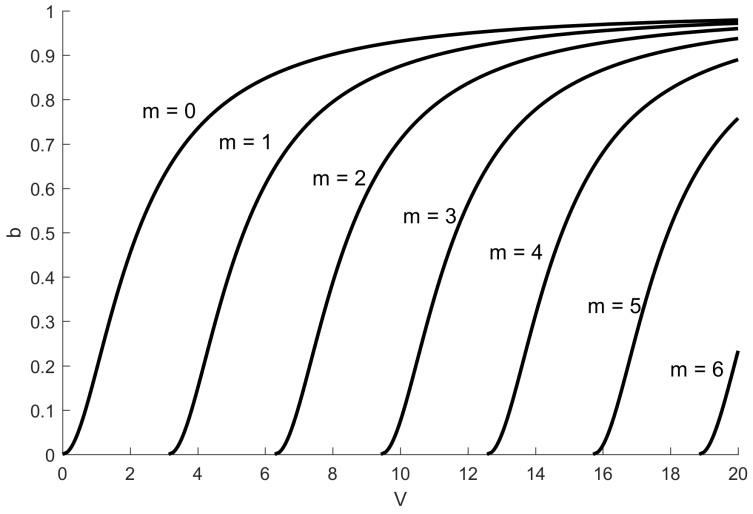

Figure 2.8: Graphic representation of b V relation for first 7 TE modes

and sought transverse propagation constants can be given by

$$\mathrm{k_{x1}} \cdot h = V\sqrt{1-b} \tag{2.103}$$

$$\mathrm{k_{x2}} \cdot h = V\ \sqrt{b} \tag{2.104}$$

Propagation constant of wave guided in central layer k_z can be derived from following equations

$$\mathrm{k_z} = \sqrt{{\mathrm{k_1}}^2 - {\mathrm{k_{x1}}}^2} = \sqrt{{\mathrm{k_{x2}}}^2 - {\mathrm{k_2}}^2} = \frac{\omega}{c}\sqrt{N} \tag{2.105}$$

Dispersion relation from (2.95) will be in final form as following

$$\frac{V\sqrt{1-b}}{2} = \tan^{-1}\sqrt{\frac{b}{1-b}} + m \cdot \pi \tag{2.106}$$

2.2.8 Transverse Magnetic Modes

We can derive dispersion relation for TM modes in very similar way. Resulting equation is identical to (2.95) with added permittivity ratio

$$\mathrm{k_{x1}} \cdot h = 2\tan^{-1}\left(\frac{\varepsilon_{r1}\mathrm{k_{x2}}}{\varepsilon_{r2}\mathrm{k_{x1}}}\right) + m \cdot \pi \tag{2.107}$$

Generalized prameters will be also very similar, however we add new parameter

$$c = \frac{\varepsilon_{r2}}{\varepsilon_{r1}} \tag{2.108}$$

Dispersion relation for generalized parameters will be

$$\frac{V\sqrt{1-b}}{2} = \tan^{-1}\frac{1}{c}\sqrt{\frac{b}{1-b}} + m \cdot \pi \tag{2.109}$$

2.2.9 Rectangular dielectric waveguide

Components of electromagnetic field for E_y modes

Previously, in slab waveguide we assumed one of the dimensions much bigger than wavelength to simplify our problem by setting $E_z = 0$ for TE mode and $H_z = 0$ for TM mode. Setting transverse dimension finite, leads to 3D solution, because electric and magnetic field is now dependent on y as well. Components E_z, H_z will be non-zero and modes are now so-called hybrid modes.

Assumption that electromagnetic wave dependency in z direction for all components of the field is still in form describing harmonic wave propagating in z direction with coefficient $e^{-jk_z z}$, where k_z is phase constant along z. If that holds true, we can then seek solution for x, y, z in the same way as before, utilizing separation of variables as in (2.78).

It is also possible to show, that one of the components of the intensity of electric wave in the transverse direction is substantially smaller than the dominant component and it is possible to omit it. Even though z component of electric field is smaller than the dominant one, we can't omit it as it is not negligible. Also if we would omit it the result would be the same solution as for slab waveguide.

Hybrid modes are often labeled by orientation of dominant component of electric field as E^x and E^y. It is further specified by two indices $E^x_{p,q}$, where $p-1$ is number of zeros in x direction and $q-1$ are zeros in y direction.

Clearly, in E^y modes E_y will be the dominant one. Assuming weakly guided wave, meaning that permittivities of all media are close, if we reduced the contrast to zero, the wave would become linearly polarized with only E_y and H_x components and rest zero. Therefore, for weakly guided waveguides, the E_x and H_y will be relatively small. For solving the problem, we first assume that H_y is negligible and with further evaluation, we will arrive to conclusion that such assumption was justified [10].

From this point, we will not be able to compare electric and magnetic field due to difference in units, so we write electric field in terms of magnetic field and unbound space impedance

$$\frac{E}{Z} = \frac{E}{Z_0}\sqrt{\varepsilon_r} \tag{2.110}$$

where Z is impedance of wave in unbound space (2.42), Z_0 in vacuum

$$Z_0 = \sqrt{\frac{\mu_0}{\varepsilon_0}} \approx 120\pi \tag{2.111}$$

This is equivalent magnetic field intensity of a wave in medium with same parameters in free space.

With assumption of H_y negligible as starting point, we can calculate the magnitude of H_x from Maxwell equation

$$\nabla \cdot \mathbf{B} = \mu_0 \nabla \cdot \mathbf{H} = 0 \tag{2.112}$$

Rewriting the divergence into components

$$\frac{\partial H_x(x,y,z)}{\partial x} + \frac{\partial H_y(x,y,z)}{\partial y} + \frac{\partial H_z(x,y,z)}{\partial z} = 0 \tag{2.113}$$

and derivating for z, where all has dependency on $e^{-jk_z z}$ and setting $H_y = 0$

$$\frac{\partial H_x(x,y,z)}{\partial x} + \underbrace{\frac{\partial H_y(x,y,z)}{\partial y}}_{0} - jk_z H_z(x,y,z) = 0 \tag{2.114}$$

we get H_z as a function of H_x

$$H_z(x,y,z) = -\frac{j}{k_z}\frac{\partial H_x(x,y,z)}{\partial x} \tag{2.115}$$

By comparing the amplitudes (not phases) of H_z, H_x in (2.115) and assuming new transverse propagation constant in x direction will arise after derivation for x, we get

$$|H_z(x,y,z)| = \frac{k_x}{k_z}|H_x(x,y,z)| \approx \frac{k_x}{k}|H_x(x,y,z)| \tag{2.116}$$

This means, that amplitude of H_z is always lower than H_x by a factor of $\frac{k_x}{k_z}$ This generally ensues from the separation to partial functions

$$\mathrm{k}^2 = \mathrm{k_x}^2 + \mathrm{k_y}^2 + \mathrm{k_z}^2 \tag{2.117}$$

According to [10] in weakly guided waveguide k_z, propagation constant for traveling wave in waveguide, is comparable to k, propagation constant for plane wave in free space with the same permittivity. Constants k_x and k_y which describe the field in transverse direction are considerably smaller. This is intuitive from the same idea of diminishing permittivity contrast, where in limit case of zero contrast, wave will not be guided and becomes plane wave, whose propagation constant $k = k_z$.

Setting amplitude of $H_x = 1$ as a reference value, than H_z will be δ times smaller (first order of δ)

$$\delta \approx \frac{k_x}{k} \ll 1 \tag{2.118}$$

Further, from adjusted Maxwell equation for wave guided in z direction we can proceed similarly as in (2.79), where after derivation for z direction, we are left with $-jkz$ and with consideration of $H_y = 0$

$$\nabla \times \mathbf{H} = \nabla \times \mathbf{H}(x,y,z) = \begin{vmatrix} \mathbf{x_0} & y_0 & z_0 \\ \frac{\partial}{\partial x} & \frac{\partial}{\partial y} & -j\ k_z \\ H_x(x,y,z) & \underbrace{H_y(x,y,z)}_{0} & H_z(x,y,z) \end{vmatrix} = j\omega\varepsilon_0\varepsilon_r\mathbf{E} \tag{2.119}$$

then

$$\mathbf{x_0}\left(\frac{\partial H_z(x,y,z)}{\partial y}\right) + y_0\left(-jk_zH_x(x,y,z) - \frac{\partial H_z(x,y,z)}{\partial x}\right) + z_0\left(-\frac{\partial H_x(x,y,z)}{\partial y}\right) = j\omega\varepsilon_0\varepsilon_r\left(\mathbf{x_0}E_x(x,y,z) + y_0E_y(x,y,z) + z_0E_z(x,y,z)\right) \tag{2.120}$$

Now we can start to evaluate each component of the field and estimate its magnitude. For E_y from (2.120) we can write

$$j\omega\varepsilon_0\varepsilon_rE_y(x,y,z) = -jk_zH_x(x,y,z) - \frac{\partial H_z(x,y,z)}{\partial x} \tag{2.121}$$

If we want to compare magnitude of amplitudes, it would be useful to modify E into form from (2.110). We achieve that by dividing with jk

$$\frac{1}{j\,k}j\omega\varepsilon_0\varepsilon_rE_y(x,y,z) = -\frac{1}{j\,k}jk_zH_x(x,y,z) - \frac{1}{j\,k}\frac{\partial H_z(x,y,z)}{\partial x} \tag{2.122}$$

and the result is

$$\frac{E_y(x,y,z)}{Z} = -\frac{k_z}{k}H_x(x,y,z) + \frac{j}{k}\frac{\partial H_z(x,y,z)}{\partial x} \tag{2.123}$$

Left side of the equation is derived as follows

$$\frac{\omega\epsilon_0\epsilon_r}{k} = \frac{1}{\frac{\omega}{c}\sqrt{\epsilon_r}}\epsilon_0\epsilon_r = \frac{1}{\sqrt{\mu_0\epsilon_0}\sqrt{\epsilon_r}}\epsilon_0\epsilon_r = \frac{\sqrt{\epsilon_r}}{\frac{\mu_0}{\epsilon_0}} = \frac{\sqrt{\epsilon_r}}{Z_0} = \frac{1}{Z} \tag{2.124}$$

When analyzing the magnitude second part of the right side in (2.123), we can notice the derivative for x. From (2.116) we will get factor δ^2 and therefore we can assume the second part negligible compared to the first component.

$$\frac{1}{k}\left|\frac{\partial H_z(x,y,z)}{\partial x}\right| \approx \frac{1}{k}\frac{\partial}{\partial x}\left|\frac{k_x}{k}\left|H_x(x,y,z)\right|\right| = \frac{{k_x}^2}{k^2}\left|H_x(x,y,z)\right| \approx \delta^2\left|H_x(x,y,z)\right| \tag{2.125}$$

Afer all, we arrive to conclusion that E_y is of the same order as H_x and can be calculated from

$$\frac{E_y(x,y,z)}{Z} = -\frac{k_z}{k}H_x(x,y,z) \tag{2.126}$$

E_y and $H_x$are therefore the main components of E^y mode.

Rest of the components are calculated very similarly [10]. From (2.120), for E_x

$$j\omega\varepsilon_0\varepsilon_r E_x(x,y,z) = -\frac{\partial H_x(x,y,z)}{\partial y} \tag{2.127}$$

divided by jk as before

$$\frac{E_x(x,y,z)}{Z} = -\frac{1}{j\ k}\frac{\partial H_x(x,y,z)}{\partial y} \tag{2.128}$$

While comparing the amplitudes we assume $k_x \approx k_y$ and therefore E_x is smaller with factor of δ^2 (2.118)

$$\left|\tfrac{E_x(x,y,z)}{Z}\right| = \frac{1}{k}\left|\tfrac{\partial H_x(x,y,z)}{\partial y}\right| = \frac{k_y}{k}\left|\tfrac{k_x}{k}\|H_x(x,y,z)\|\right| = \frac{k_x k_y}{k^2}\left|H_x(x,y,z)\right| = \delta^2\left|H_x(x,y,z)\right| \tag{2.129}$$

component E_x is therefore negligible in T^y mode. Lastly, E_z from (2.120)

$$j\omega\varepsilon_0\varepsilon_r E_z(x,y,z) = -\frac{\partial H_x(x,y,z)}{\partial y} \tag{2.130}$$

divided by jk again

$$\frac{E_z(x,y,z)}{Z} = -\frac{1}{j\,k}\frac{\partial H_x(x,y,z)}{\partial y} \tag{2.131}$$

and in form as before

$$\left|\frac{E_z(x,y,z)}{Z}\right| = \left|\frac{1}{k}\frac{\partial H_x(x,y,z)}{\partial y}\right| = \frac{k_y}{k}\left|H_x(x,y,z)\right| \approx \delta\left|H_x(x,y,z)\right| \tag{2.132}$$

we can see that E_z is smaller by factor of δ.

To summarize, when evaluating E^y mode, we take E_y and H_x as main components, next we consider E_z and H_z smaller with factor δ and omit E_x and H_y smaller with factor δ^2 than reference values.

2.2.10 Rectangular waveguide with E^y modes calculation

In previous section we derived, that rectangular waveguide with E^y modes has E_y, H_x, E_z, H_z components and all of them are possible to write in terms of H_x. From Marcatili method [13], we can mark rectangular areas above and next to inner part of the waveguide and write their equations, viz. Figure 2.9a. Areas around corners are ignored. Boundary conditions are assumed to be unchanging along the interface and the effect of corners is again neglected. Setting both horizontal and vertical outer areas with the same permittivity, we can solve the field distribution only for the top and right side (x, $y > 0$) and take advantage of symmetricity. In the inner section of the waveguide, traveling wave with coefficient k_z and standing wave in transverse direction x, y is formed. Solution is similar to (2.83), but now add distribution along the y axis as well. Solving these partial functions always leads to sum of sine and cosine, so even and odd solution respectively [13]. We evidently can rewrite it using complex exponential as well

$$\mathrm{H}_{x1}(x,y,z) = \mathrm{C}_1\cos(\mathrm{k_{x1}}\cdot x + \phi_{x1})\cos(\mathrm{k_{y1}}\cdot y + \phi_{y1})e^{-j\mathrm{k_z}\cdot z} \tag{2.133}$$

In are 2 above the core, field distribution will be in a form of evanescent wave, in layer below, symmetrical relationship hold true

$$\mathrm{H}_{x2}(x,y,z) = \mathrm{C}_2\cos(\mathrm{k_{x2}}\cdot x + \phi_{x2})e^{-\mathrm{k}_{y2}\cdot y}\,e^{-j\mathrm{k_z}\cdot z} \tag{2.134}$$

Form of these equations comes from boundary condition of the traveling and standing wave along the x axis, thus the same cosine function for x and complex exponential for z.

In section 3 on the right side, we have equivalent solution

$$\mathrm{H}_{x3}(x,y,z) = \mathrm{C}_3 \cos(\mathrm{k_{y3}} \cdot y + \phi_{y3}) e^{-\mathrm{k}_{x3} \cdot x}\ e^{-j\mathrm{k_z} \cdot z} \tag{2.135}$$

For interface between 1 and 2 we know, that to satisfy boundary conditions, following constants have to be equal

$$\mathrm{k_{x1}} = \mathrm{k_{x2}} = \mathrm{k_x}, \qquad \phi_{\mathrm{x1}} = \phi_{\mathrm{x2}} = \phi_{\mathrm{x}} \tag{2.136}$$

Analogically for interface 1 and 3

$$\mathrm{k_{y1}} = \mathrm{k_{y3}} = \mathrm{k}_y, \qquad \phi_{\mathrm{y1}} = \phi_{\mathrm{y3}} = \phi_y \tag{2.137}$$

Equations are simplified into

$$\mathrm{H}_{x1}(x,y,z) = \mathrm{C}_1 \cos(\mathrm{k_x} \cdot x + \phi_x) \cos(\mathrm{k_y} \cdot y + \phi_y) e^{-j\mathrm{k_z} \cdot z} \tag{2.138}$$

$$\mathrm{H}_{x2}(x,y,z) = \mathrm{C}_2 \cos(\mathrm{k_x} \cdot x + \phi_x) e^{-\mathrm{k}_{y2} \cdot y}\ e^{-j\mathrm{k_z} \cdot z} \tag{2.139}$$

$$\mathrm{H}_{x3}(x,y,z) = \mathrm{C}_3 \cos(\mathrm{k_y} \cdot y + \phi_y) e^{-\mathrm{k}_{x3} \cdot x}\ e^{-j\mathrm{k_z} \cdot z} \tag{2.140}$$

Next we can set the boundary conditions on the two interfaces. For these conditions to be satisfied, tangential component of intensity of electric field E and tangential component of magnetic field H have have to be the same on the interface. Equivalently, same holds true for normal components of electric induction D and magnetic induction B.

First, we take a look at the top boundary between 1 and 2. For tangential components of E_z, H_x, E_z, H_z [13]

$$H_x(x,y,z) \tag{2.141}$$

$$E_z(x,y,z) = \frac{j}{j\omega\varepsilon_0\varepsilon_r} \frac{\partial H_x(x,y,z)}{\partial y} \tag{2.142}$$

$$H_z(x,y,z) = -\frac{j}{k_z} \frac{\partial H_x(x,y,z)}{\partial x} \tag{2.143}$$

and for normal components of E_z, H_x, E_z, H_z

$$D_y(x,y,z) = \varepsilon_0\varepsilon_r E_y(x,y,z) = \frac{-k_z}{\omega} H_x(x,y,z) \tag{2.144}$$

From these equations it is possible to see that if values at boundary of (2.141) $H_x(x, y, z)$ and (2.142)

$$H_x(x, y, z) = \frac{1}{\varepsilon_r} \frac{\partial H_x(x, y, z)}{\partial y}, for y = h/2 \tag{2.145}$$

are equal, the rest components will be equal automatically. Next we can apply conditions from (2.145) to find field components at upper interface for $y = h/2$, for H_x from (2.138), (2.139)

$$\mathrm{C}_1 \cos(\mathrm{k_y} \cdot \frac{h}{2} + \phi_y) = \mathrm{C}_2 e^{-\mathrm{k}_{y2} \cdot \frac{h}{2}} \tag{2.146}$$

$$\frac{1}{\varepsilon_{r1}} \frac{\partial H_{x1}(x, y, z)}{\partial y} = \frac{1}{\varepsilon_{r2}} \frac{\partial H_{x2}(x, y, z)}{\partial y} \tag{2.147}$$

then

$$-\frac{\mathrm{k_y}}{\varepsilon_{r1}} \mathrm{C}_1 \sin(\mathrm{k_y} \cdot \frac{h}{2} + \phi_y) = -\frac{\mathrm{k}_{y2}}{\varepsilon_{r2}} \mathrm{C}_2 e^{-\mathrm{k}_{y2} \cdot \frac{h}{2}} \tag{2.148}$$

Dividing (2.148) and (2.146), we apply the same process as before for slab waveguide, we eliminate constants C

$$\tan(\mathrm{k_y} \cdot \frac{h}{2} + \phi_y) = \frac{\varepsilon_{r1}}{\varepsilon_{r2}} \frac{\mathrm{k}_{y2}}{\mathrm{k_y}} \tag{2.149}$$

Plugging $y = -h/2$ for lower boundary, we get very similar result as (2.149)

$$\tan(\mathrm{k_y} \frac{h}{2} - \phi_y) = \frac{\varepsilon_{r1}}{\varepsilon_{r2}} \frac{\mathrm{k}_{y2}}{\mathrm{k_y}} \tag{2.150}$$

Rewriting (2.149) and (2.150) and putting them together, we get dispersion relation to one half of the solution for unknown constant k_y and k_{y2}

$$\mathrm{k_y} h = 2\tan^{-1}\left(\frac{\varepsilon_{r1}}{\varepsilon_{r2}} \frac{\mathrm{k}_{y2}}{\mathrm{k_y}}\right) + q\,\pi \tag{2.151}$$

We can notice that the resulting relation is completely identical to (2.107), representing TM mode in 2D waveguide. Here we define it as so called W waveguide [13], viz. Figure 2.9b Applying the same procedure for side boundary, we come to a conclusion that resulting dispersion relation is identical to TE mode in 2D waveguide (2.95), viz. Figure 2.9c

$$\mathrm{k}_x w = 2\tan^{-1}\left(\frac{\mathrm{k}_{x2}}{\mathrm{k}_x}\right) + p\,\pi \tag{2.152}$$

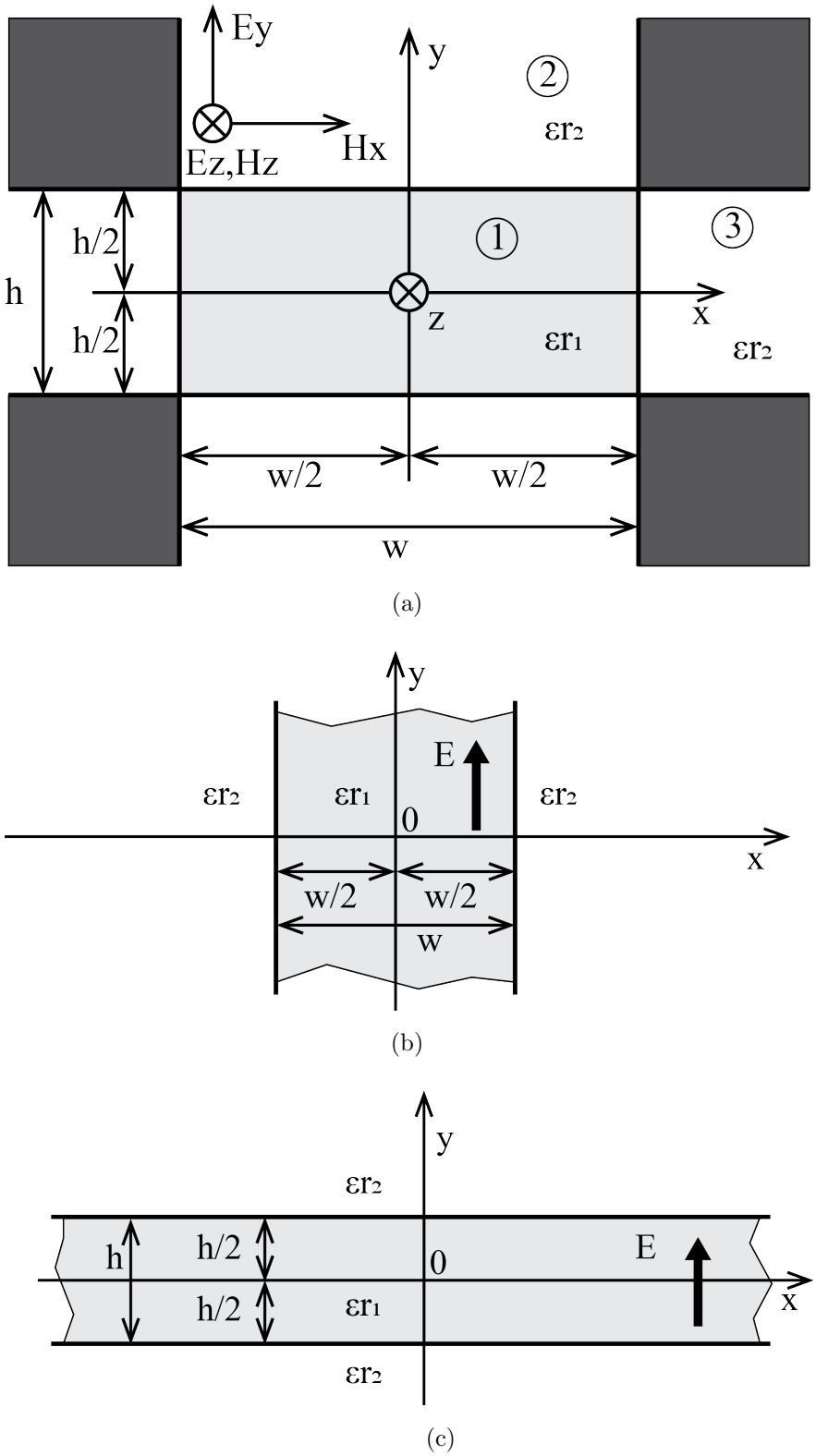

Figure 2.9: (a) Diagram of rectangular waveguide with core width w height h, core and cladding permittivity ϵ_{r1}, ϵ_{r2} respectively, (b) equivalent 2D waveguide W, (c) equivalent waveguide H, images redrawn from [10]

2.2.11 1-D periodic structure

From the theory of quantum mechanics, we know that electrons can propagate through perfect crystal lattice periodic potential as waves, without scattering if they meet certain criteria. However, such lattice can also prevent propagation of waves of certain energy level in a certain direction. This phenomenon is described as energy band gaps (forbidden bands) in the band structure of solids. Having strong enough potential, the crystal lattice forbidden gap can and prevent propagation in all directions and forming a complete band gap. An example of complete bandgap could be in semiconductor, between valence and conductive energy bands. Analogically, structures with a periodical arrangement of differing dielectric constants (or index of refraction) can exhibit similar behavior for photons. If the difference in dielectric constants is adequate and the material loss is small we can produce a lot of the same phenomena as electrons show in the crystal. One of the main uses for such periodic structures is a formation of photonic band gaps - restricting propagation and reflecting certain wavelength band. Quarter wave stack, also known by may more names, such as distributed Bragg reflector, Bragg grating, one-dimensional photonic crystal, consists of stacked layers of material with alternating reflective index. An incident light wave of an appropriate wavelength corresponding to the structure period is in part reflected at each interface. If the structure is periodical the multiple reflections destructively interfere with propagating wave and thus eliminate it. This principle is utilized in many present-day devices, such as Distributed Feedback Lasers, fiber grating filters and Bragg assisted contra-directional couplers to name but a few. All of these structures are periodical in one dimension, therefore by definition, they are called one-dimensional photonic crystals.

Reciprocal lattice is defined as Fourier transform of a lattice. Lattice is a periodic spatial function also called direct lattice. If we define

$$f(r)$$

as a periodic function on such lattice, then

$$f(r) = f(r + R)$$

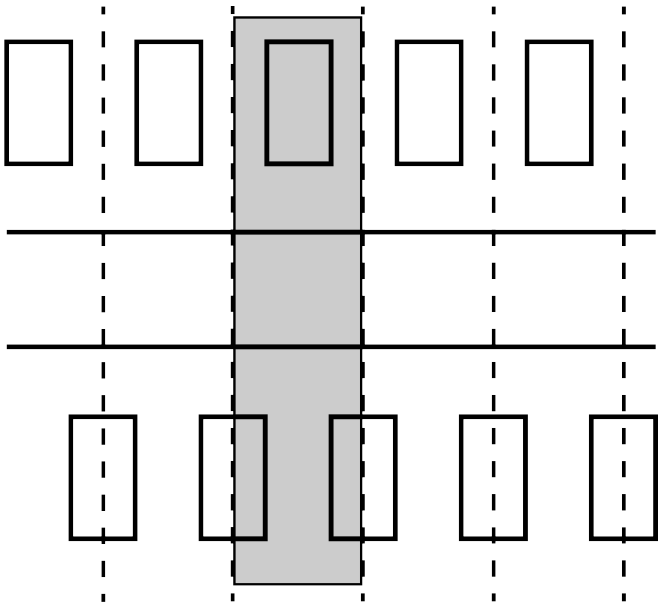

Figure 2.10: Wigner-Seitz cell of proposed contra-directional coupled structure

where

$$R$$

is so called lattice vector and it translates the lattice onto itself [14]. Given reciprocal lattice, we can define unit cell sized one period called Wigner–Seitz cell or first Brillouin zone.

Schematic of Wigner-Seitz cell of contra-directional coupler structure is shown in 2.10

2.3 Coupled Mode Theory, Perturbation Theory

Many structures can be derived from coupled mode theory, including filters, co- and contra-directional couplers with and without periodic perturbation, etc. Let's consider two electromagnetic modes with complex amplitudes A and B and propagation constants β_1 and β_2.

$$\mathbf{E_a}(x,z) = A \cdot \exp -j\beta_1 z \mathbf{E_b}(x,z) = B \cdot \exp -j\beta_2 z \tag{2.153}$$

where A and B are constant.

Faced with perturbation, such as periodic field or waveguide corrugation, power is partially or fully exchanged between the modes. In such case, the modes amplitude A and B is no longer constant but they will be dependent on propagation, z, direction

$$\frac{dA}{dz} = \kappa_{12} B \exp^{-j\delta\beta z} \tag{2.154}$$

$$\frac{dB}{dz} = \kappa_{21} A \exp^{-j\delta\beta z} \tag{2.155}$$

where κ_{12} and κ_{21} are coupling coefficients are derived from physical structure under consideration, $\delta\beta$ is detuning parameter depending on both β_1, β_2 and spatial characteristic of the perturbation. There are couple situations

2.3.1 Co-directional Coupling

In case of co-directional coupling, modes $\mathbf{E_a}$ and $\mathbf{E_b}$ propagate in the same direction. If we set $|A|^2$ and $|B|^2$ to be equal to the power of the modes $\mathbf{E_a}$ and $\mathbf{E_b}$ respectively, the we can express power conservation over propagation direction z as

$$\frac{d}{dz}(|A|^2 + |B|^2) = 0 \tag{2.156}$$

it can be shown, that this is satisfied for

$$\kappa_{12} = -\kappa_{21}^* \tag{2.157}$$

Then, if we set initial conditions so one mode is incident on the structure in $z = 0$ while the other is zero

$$E_a(0) = A_0 \qquad\qquad E_b(0) = 0 \tag{2.158}$$

Then solution to (2.154) is

$$A(z) = A_0 e^{-j\frac{\delta\beta z}{2}} \left[\cos\left(\frac{1}{2}\sqrt{4\kappa^2 + \delta\beta^2} \cdot z \right) - j\frac{\delta\beta}{\sqrt{4\kappa^2 + \delta\beta}} \sin\left(\frac{1}{2}\sqrt{4\kappa^2 + \delta\beta^2} \cdot z \right) \right] \tag{2.159}$$

$$B(z) = A_0 \frac{2\kappa_{ab}}{\sqrt{4\kappa^2 + \delta\beta}} e^{-j\frac{\delta\beta z}{2}} \sin\left(\frac{1}{2}\sqrt{4\kappa^2 + \delta\beta^2} \cdot z\right) \tag{2.160}$$

where $\kappa = |\kappa_{12}|$. When $\delta\beta = 0$, the phase matching condition is satisfied and power is fully transferred between the modes with spatial periodicity. Modes can them be written as

$$E_a(z) = A_0 e^{-i\beta z} \cos(\kappa z) \tag{2.161}$$

$$E_b = A_0 \frac{\kappa_1 2}{\kappa} e^{-i\beta z} \sin(\kappa z) \tag{2.162}$$

2.3.2 Contra-directional Coupling

Contra-directional coupling principle is used for device design in this work, therefore more attention is paid to this subject. Bragg grating assisted contra-directional couplers (CDC) are extensively utilized as wavelength selective add-drop filters. Conventional CDC consists of 2 dissimilar waveguides and periodic perturbation realized either by corrugating waveguide sidewalls or the slab between waveguides. Due to the waveguide asymmetry, there is little to no conventional directional coupling and contra-directional coupling is utilized instead. The Bragg grating matches the phase and provides necessary momentum for coupling the forward propagating mode in one waveguide into the backwards propagating mode in the other. There are two conditions allowing for mode coupling - direct Bragg coupling and exchange Bragg coupling.

Direct coupling occurs between modes of the same waveguide and it is a coupling of forward propagating mode back into the backwards propagating mode, caused by constructive reflection by Bragg grating. It occurs when one of the following conditions is satisfied [15]:

$$2\beta_1(\omega_1) = (2\pi)/\Lambda \qquad 2\beta_2(\omega_2) = (2\pi)/\Lambda \tag{2.163}$$

where β_1, β_2 are the propagation constants of first and second mode of the coupler structure, ω_1 ,ω_2 are central frequencies of reflected light, and Λ is grating period. This causes back reflection, limits spectral range of coupler and is

therefore unwanted. To increase free spectral range $\omega_2 - \omega_1$ high asymmetry is usually required.

In the proposed structure, showed in , input waveguide with multiple wavelengths is simple strip waveguide containing no perturbations, therefore will be very little back reflection. Nevertheless, there still will be back reflection from the subwavelength waveguide at wavelength

$$\beta_2 = \frac{\pi}{\Lambda} \tag{2.164}$$

In exchange coupling, mode of the first waveguide is reflected and coupled into back-propagating mode of second waveguide. Bragg exchange condition is as follows[15]:

$$\beta_1(\omega) + \beta_2(\omega) = (2\pi)/\Lambda \tag{2.165}$$

where ω is reflection central frequency. In this case Bragg grating is providing necessary momentum to transfer first (forward propagating) mode into second (contra-directional) mode.

This approach is approximation with assumption of big separation of the coupled waveguides and therefore orthogonality of the propagated modes. Now we define four modes of the structure, with amplitudes A_i and B_i where $i = 1, 2$ corresponding to waveguide 1 and 2. Amplitudes denoted with A are of forward propagated modes and B are of backward propagated modes. Electric field in the structure can therefore be expressed as

$$\mathbf{E} = \left(A_1(z)e^{-j\beta_1} + B_1 e^{j\beta_1}\right) \cdot U_1(x) + \left(A_2(z)e^{-j\beta_2} + B_2 e^{j\beta_2}\right) \cdot U_2(x) \tag{2.166}$$

where β_1, β_2 are propagation constants of waveguide 1 and 2 respectively, and U_1, U_2 are transverse distributions of electromagnetic field. The mode amplitudes are z dependent, due to the coupling introduced by Bragg grating.

Chapter 3

Device Design and Description

3.1 Device characterization and analytical approximation

From contra-directional phase matching condition (2.165), we can predict several ways to adjust center wavelength. First, on the left side of the equation, there are propagation constants of the two waveguides in the structure. By changing the dimensions of the strip waveguide, effective index of refraction is modified and therefore propagation changes. In this work, we use relatively narrow strip waveguide and thus the light is not perfectly confined in the core and we can expect notable change with the change of the width. Propagation constant of subwavelength waveguide can be changed either bu changing its dimensions, as in strip waveguide, or by changing its duty cycle. In this work, modulation of duty cycle is not investigated due to possible difficulties later in fabrication process. Since light is much less confined than in traditional waveguide, the change of effective index with change of dimensions is expected to be much less pronounced. Lastly, we can adjust the Bragg reflection condition by varying the pitch of the SWG. Pitch has traditionally strong effect on the reflected waveguide.

3.1.1 Demultiplexer Overall Design

The demultiplexer block schematic is shown in Figure 3.2. It is comprised of Mach-Zehnder Interferometer (MZI), and four channel dropping segments. MZI is a band pass filter to separate the 8 channels (L0 - L7) into 2 groups of 4 (L0 - L3 and L4 - L7), each group continues to contra-directional coupler segments. There are 2 segments in each branch and each segment is able to drop 2 channels. To ensure good separation of dropped channels and to limit crosstalk, each segment drop either odd or even channels, i.e. first segment in upper branch drops channel L0 and L2, the second one L1 and L3 and analogically in the lower branch. Input and output signals are coupled by Bragg grating couplers.

3.1.2 Mach-Zehnder Interferometer

Schematic of Mach-Zehnder interferometer schematic is in Figure 3.1. It consists of 3 directional couplers, C1, C2 and C3 with coupling length $CL1 = 7.03\mu m$, $CL2 = 4.27\mu m$ and $CL3 = 1.73\mu m$respectively, coupler gap $g = 0.2\mu m$ and waveguide width $w = 0.32\mu m$. Interferometer arms M1 and M2, longer arm comprised of 4 quarter circle segments with radius $r = 6\mu m$ and length adjusting segments $a1 = 0\mu m$ and $a2 = 10\mu m$. Arm difference is therefore $\Delta l_1 = (2\pi r + 2a_1) - 4r$ and $\Delta l_2 = 2\Delta l_1$.

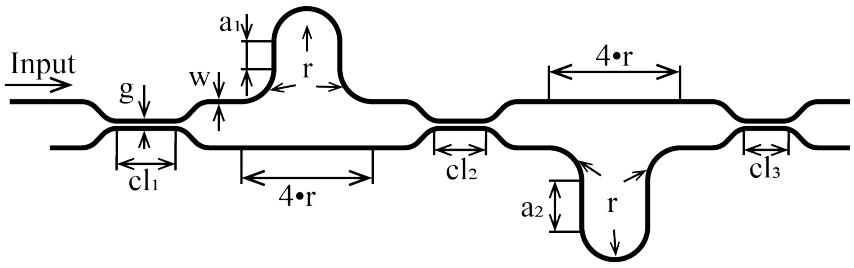

Figure 3.1: Schematic of 2 stage Mach-Zehnder interferometer bandpass filter

First stage of Mach-Zehnder interferometer was simulated and optimized to set the $-3dB$ band crossing to the LAN-WDM empty channel at $230.6THz(1300.05\mu m)$. Result is plotted in Figure

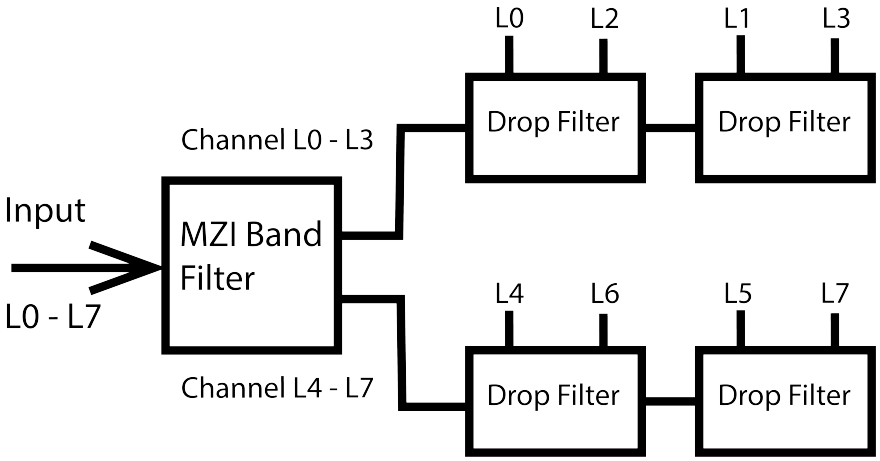

Figure 3.2: Block diagram of de/multiplexer

3.1.3 Contra-Directional Coupler Segment

The schematic of contra-directional coupler segment is in Figure 3.4. It consists of throughput channel (T) with width W_{T} and two drop channels on each side(D_1 and D_2) with width W_{D1} and W_{D2}. G_1 and G_2 are gaps between T and D_1, D_2 respectively. Throughput channel T is strip waveguide and drop channels D_1 and D_2 are subwavelength waveguides with pitch $\Lambda_{\mathrm{D1}} = \Lambda_{\mathrm{D2}} = 340nm$, number of periods $N_{\mathrm{D1}} = N_{\mathrm{D2}} = 1300$ and duty cycle $DC = 50\%$. Cladding for the whole device is $Si0_2$. The height of all waveguides is 220nm, as a standard in SOI technology for passive optical devices. W_{T} was chosen 280nm, W_{D1} and W_{D2} are variable to adjust demultiplexing channels. Subwavelength waveguides are shifted relative to each other by $\Lambda/2$ to minize their mutual interaction and thus reduce crosstalk.

In the last 50 periods of the segmented waveguide D_1 and D_2, taper is realized to couple light into conventional strip waveguide P_1 and P_2 [16]. Waveguides W_{D1} and W_{D2} are linearly decreased over the 50 periods until the widths match. In last 10 periods, bridging elements are introduced to help make the mode transition smoother. Width of these elements is increasing from 150nm to W_{P1} or W_{P2}. Taper is linearly chirped to period of 300nm.

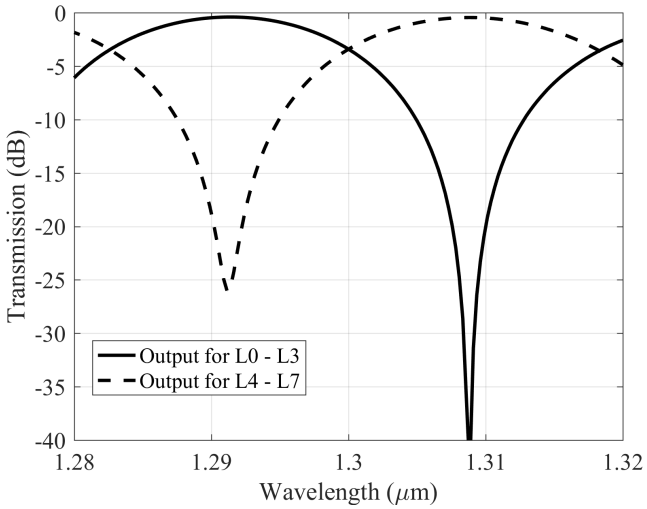

Figure 3.3: Simulated spectrum of first stage of Mach-Zehnder interferometer with -3 dB band crossing at $230.6THz(1300.05\mu m)$ corresponding to empty channel of proposed LAN-WDM grid

3.1.4 Apodization

Bragg reflector is an attractive solution for integrated filters. However, Bragg grating on its own doesn't have sufficient spectral properties such as large side lobes, which is undesirable. Side lobes are a result of reflections from ends of the grating and making Fabry-Perot resonator and in contra-directional coupler, they cause crosstalk between adjacent channels. Apodization of Bragg grating structures is a gradual modification of perturbations along the length of the structure. Modulating coupling coefficient is an effective way of suppressing the side lobes. There are number different ways practical realization, i.e. sampled grating [17] varying etch depth or perturbation size for side wall corrugated waveguide [1]. Lastly, for contra-directional coupler, there is the possibility to control coupling coefficient by modulating gap between through and drop waveguide. It has been shown that for best results Gaussian profile of coupling coefficient is recommended.

Each segment of SWG is shifted in transverse direction over longitudinal direc-

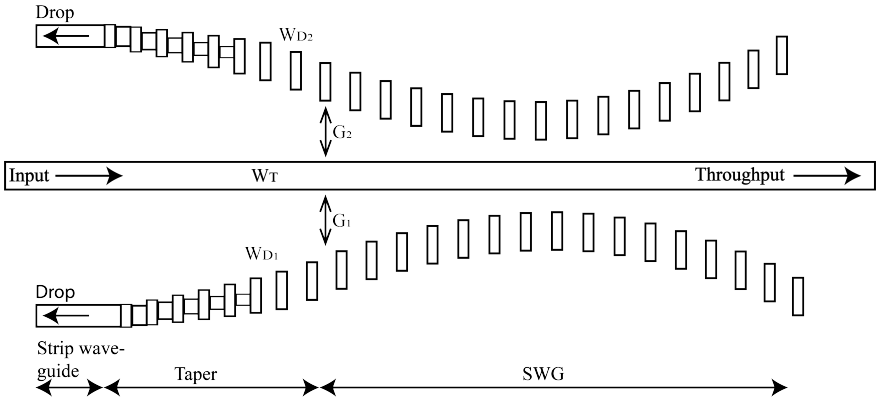

Figure 3.4: Schematic of Drop Channel Segment

tion. Gaussian distribution can be expressed

$$f(z) = A \cdot e^{-\frac{(z-Z_0)^2}{2c^2}} \tag{3.1}$$

where A is the amplitude, Z_m is maximum length, and c is variance, giving shape of the curve.

Therefore x coordinate of ith segment of SWG is given by

$$x_i(i) = x_{max} \cdot e^{-\frac{(i-N/2)^2}{2c^2}} - x_{max} - G \tag{3.2}$$

where x_i is x position of ith segment, x_{max} is magnitude of the apodization, N number of periods, c variation parameter, and G is the smallest gap between the center waveguide and SWG. The gap in the center of the structure is varied from $0.36\mu m$ to $0.42\mu m$ to account for increasing reflection bandwidth with increasing center wavelength.

3.1.5 Analytical approach utilizing Marcatili method and Coupled Mode Analysis

To analytically describe our design of contradirectional coupler, Marcatili method derived before was utilized. To employ Marcatili and Coupled Mode Analysis, subwavelength waveguide had to be approximated by a rectangular waveguide. However, it has proven very difficult to accommodate all properties of SWG using only one equivalent waveguide. For example, if we match propagation

constant, the electric field will be much more confined inside the waveguide, limiting coupling coefficient between the waveguides. Furthermore, it will be shown, that using basic formula to calculate effective index of refraction of SWG from [18]

$$n_{eff} = \sqrt{\cdot}(Dn_1^2 + (1 - D) \cdot n_2^2) \tag{3.3}$$

will not give appropriate results, since it doesn't take transverse dimensions into account. With these considerations taken into account, subwavelength waveguide was approximated by two different waveguides, first, for propagation constant calculation and second for mode profile to be used in coupling coefficient estimation.

Calculation of waveguide parameters for center strip waveguide

The central strip waveguide has known dimensions width $w = 280nm$ and height $h = 220nm$, relative permittivities of core $\epsilon_r 1 = n_1^2 = 12.2$ and cladding $\epsilon_r 2 = n_2^2 = 2.1025$.

First, we calculate propagation constant in y axis, the H waveguide.

Taking equation from (2.151)

$$\mathrm{k_y} h = 2\tan^{-1}\left(\frac{\varepsilon_{r1}}{\varepsilon_{r2}}\frac{\mathrm{k_{y2}}}{\mathrm{k_y}}\right) \tag{3.4}$$

and rewriting for k_{y2}

$$\mathrm{k_{y2}} = k_y \frac{\epsilon_r 2}{\epsilon_r 1}\tan\left(\frac{\mathrm{k}_y h}{2}\right) \tag{3.5}$$

Using basic relations

$$k_y = \sqrt{k_1^2 + k_{zH}^2}, k_{y2} = \sqrt{k_{zH}^2 - k_1^2} \tag{3.6}$$

where $k_z H$ is sought propagation constant.

Adding equations from (3.6), we can eliminate $k_z H$ and get following relation

$$sqrtk_y^2 + k_{y2}^2 = \sqrt{k_1^2 - k_2^2} = \frac{\omega}{c}\sqrt{\epsilon_r 1^2 - \epsilon_r 2^2} \tag{3.7}$$

Plugging (3.5) to (3.7)

$$sqrtk_y^2 + k_{y2}^2 = sqrtk_y^2 + \left[k_y \frac{\epsilon_r 2}{\epsilon_r 1} \tan\left(\frac{\mathrm{k}_y h}{2}\right)\right]^2 = \frac{\omega}{c}\sqrt{\epsilon_r 1^2 - \epsilon_r 2^2} \tag{3.8}$$

From Equation (3.8) we get transcendental equation for k_y which we have to solve numerically

$$sqrtk_y^2 + \left[k_y \frac{\epsilon_r 2}{\epsilon_r 1} \tan\left(\frac{\mathrm{k}_y h}{2}\right)\right]^2 = \frac{\omega}{c}\sqrt{\epsilon_r 1^2 - \epsilon_r 2^2} \tag{3.9}$$

For $\omega = 230.6THz(1.3\mu m)$ and previously stated aterial and dimensional parameters, we get

$$k_y = 10.153 \cdot 10^6 \frac{1}{m} \tag{3.10}$$

Having found k_y, we can now calculate propagation constant for H waveguide

$$k_{Hz} = \sqrt{k_1^2 - k_y^2} = 13.531 \cdot 10^6 \tag{3.11}$$

where $k_1 = k_0\sqrt{\epsilon_r 1}$ and $k_0 = \frac{\omega}{c}$ is free space propagation constant.

Propagation constant for equivalent W waveguide can be obtained in similar way from dispersion relation for TE mode, viz. (2.152)

$$\mathrm{k}_x w = 2\tan^{-1}\left(\frac{\mathrm{k}_{x2}}{\mathrm{k}_x}\right) \tag{3.12}$$

again rewrite for k_{x2}

$$\mathrm{k}_{x2} = \mathrm{k}_x \tan\left(\frac{\mathrm{k}_x w}{2}\right) \tag{3.13}$$

basic equations for W waveguide propagation constant

$$\mathrm{k_x} = \sqrt{\mathrm{k_1}^2 - \mathrm{k_{zW}}^2}, \mathrm{k}_{x2} = \sqrt{\mathrm{k_{zW}}^2 - \mathrm{k_2}^2} \tag{3.14}$$

adding them together

$$\sqrt{\mathrm{k_x}^2 + \mathrm{k}_{x2}{}^2} = \sqrt{\mathrm{k_1}^2 - \mathrm{k_2}^2} = \frac{\omega}{c}\sqrt{\varepsilon_{r1} - \varepsilon_{r2}} \tag{3.15}$$

substituting for k_{x2} we get transcendental equations for k_x

$$\sqrt{\mathrm{k_x}^2 + \left[\mathrm{k}_x \tan\left(\frac{\mathrm{k}_x w}{2}\right)\right]^2} = \frac{\omega}{c}\sqrt{\varepsilon_{r1} - \varepsilon_{r2}} \tag{3.16}$$

and numerically solved

$$k_x = 8.77 \cdot 10^6 \frac{1}{m} \tag{3.17}$$

and finally, propgation constant k_{zW} of W waveguide

$$\mathrm{k_{zW}} = \sqrt{\mathrm{k_1}^2 - \mathrm{k_y}^2} = 14.465 \cdot 10^6 \frac{1}{m} \tag{3.18}$$

Combining k_{zH} and k_{zW} we get total propagation constant of the calculated waveguide

$$\mathrm{k_z} = \beta = \sqrt{\mathrm{k_{zH}}^2 + \mathrm{k_{zW}}^2 \text{ - } \mathrm{k_y}^2} = \sqrt{\mathrm{k_1}^2 - \mathrm{k_x}^2 - \mathrm{k_y}^2} = 10.304 \cdot 10^6 \frac{1}{m} \tag{3.19}$$

Approximation of propagation constant of subwavelength waveguide

Previously referenced formula for estimating effective refractive index [18] $n_{eff} = \sqrt{D \cdot n_{core}^2 + (1 - D) \cdot n_{clad}^2}$ requires slabs with infinite transverse dimensions and thus yields substantial error for narrow SWGs. The electric field in high-index part of SWG isn't completely confined and the electric wave will propagate with an effective index of refraction lower than the index of refraction of the high-index material. Therefore, we propose to calculate the approximate effective index of SWG with the following edit

$$n_{eff} = \sqrt{D \cdot n_{effwg}^2 + (1 - D) \cdot n_{clad}^2} \tag{3.20}$$

where n_{effwg} is an effective index of refraction of the equivalent rectangular waveguide with same transverse dimensions.

We can now compare approximations and numerical solution of the propagation constants. Four methods were employed. The first method is analytical, calculating the equivalent waveguide effective index from propagation constant obtained by Marcatili method described before

$$n_{effwg} = \frac{\beta}{k_0} \tag{3.21}$$

and plug in (3.20).

Second, similarly as the first method, but we use Lumerical FDE solver to obtain

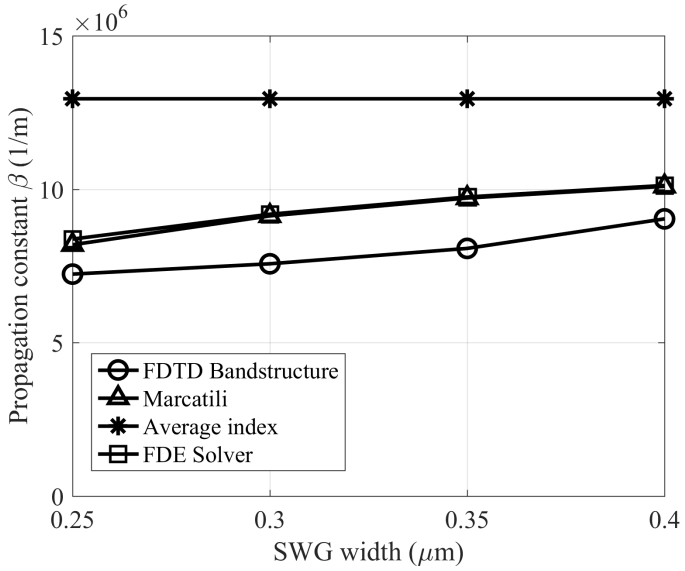

Figure 3.5: Comparison of subwavelength waveguide effective index of refraction approximation to numerical method for SWG width from $0.25\mu m$ to $0.4\mu m$ and frequency $f = 230.6THz$

the equivalent waveguide effective index. Third, the approximate average is calculated by the formula from [18]. Lastly, we compare all the approximations to propagation constant of SWG directly calculated in Lumerical FDTD Solutions by bandstructure simulation.

In Figure 3.5 we can see the resulted propagation constants for SWG width from $0.25\mu m$ to $0.4\mu m$ and frequency $f = 230.6THz$. The method of averaging material yields the biggest difference compared to numerical bandstructure simulation and doesn't show the relationship between the width of SWG and its propagation constant. Proposed new method closely follows the rising trend seen in numeric simulation. Difference between approximations and the simulation can be seen in Figure 3.6

Average index of refraction method shows as much as 80% difference for SWG width $0.25\mu m$ and around 40% for $0.4\mu m$, whereas proposed method of calculation is better than 20% for all widths. This new method of calculating the effective refractive index of the subwavelength waveguide will be of great use for analytically describing proposed contra-directional coupler structure.

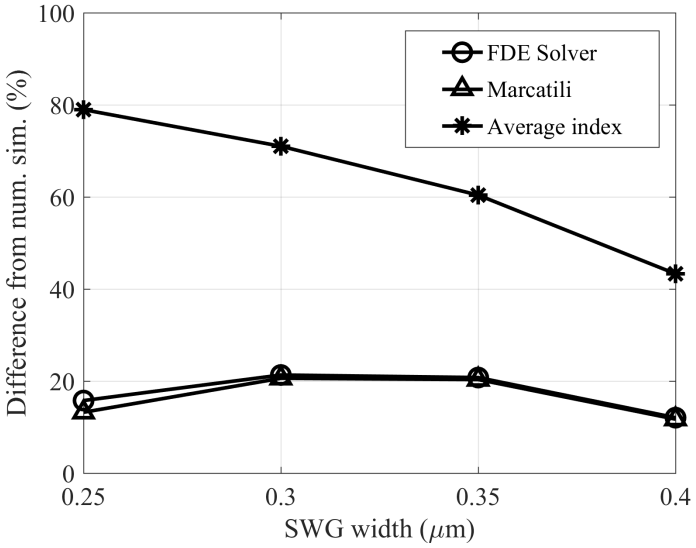

Figure 3.6: Difference between simulation and calculated approximation of SWG effective refractive index

Calculating central wavelengths of signal transmission

Having both, central waveguide and SWG, analytically described, we can calculate propagation constants for any chosen waveguide dimension and frequency. In propagation constants for strip waveguide of width $w = 280nm$ and four SWG widths $w1 = 250nm$,$w2 = 300nm$,$w3 = 350nm$,$w4 = 400nm$ are plotted.

To get desired frequency of power transmission, we can graphically display contra-directional coupling condition

$$\beta_{SWG} + \beta_{WG} = k_{reflected} \tag{3.22}$$

where β_{SWG} and β_{WG} are propagation of subwavelength waveguide and strip waveguide respectively. $k_{reflected} = \frac{2\pi}{\Lambda}$ is Bragg reflection condition and $\Lambda = 340nm$ chosen period of SWG, in our case we calculate with 340nm. In Figure we can see propagation constant sum of each SWG with strip waveguide giving us left side of equation (3.22) and line $k_{reflected} = 18.48 \cdot 10^6(1/m)$ representing right side of (3.22). Crossing of the lines means fulfillment of condition (3.22) and transmission of energy from strip waveguide to SWG.

Finally, we can plot the resulting transmission frequencies, converted to wavelengths for convenience, against SWG width, viz. Figure 3.9.

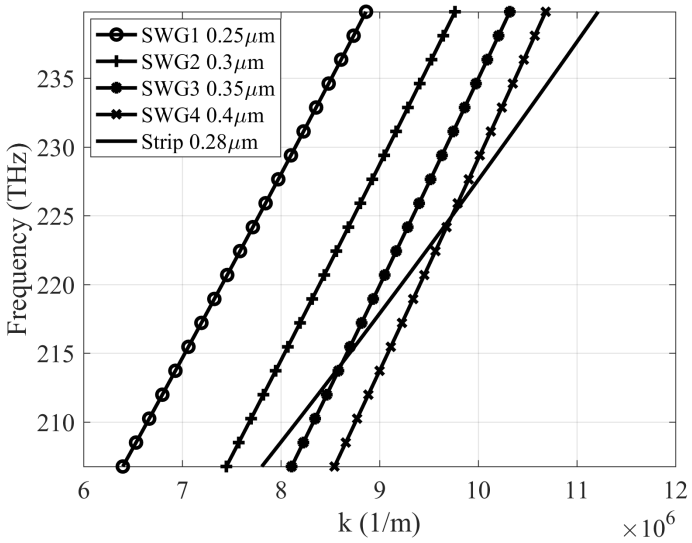

Figure 3.7: Calculated propagation constants for four different SWGs and one strip waveguide. Widths of SWGs are $SWG_1 = 250nm$, $SWG_2 = 300nm$, $SWG_3 = 350nm$, $SWG = 400nm$, strip waveguide width is $280nm$

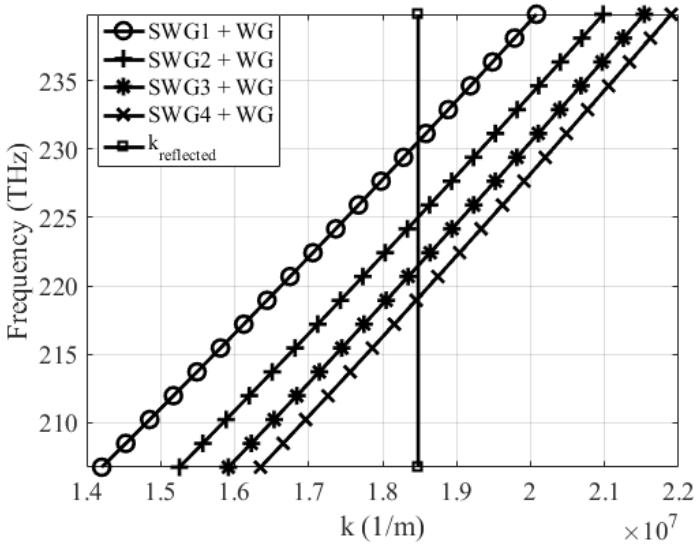

Figure 3.8: Graphical representation of contra-directional coupling condition (3.22) for four SWGs $SWG_1 = 250nm$, $SWG_2 = 300nm$, $SWG_3 = 350nm$, $SWG_4 = 400nm$ and strip waveguide WG with width $280nm$

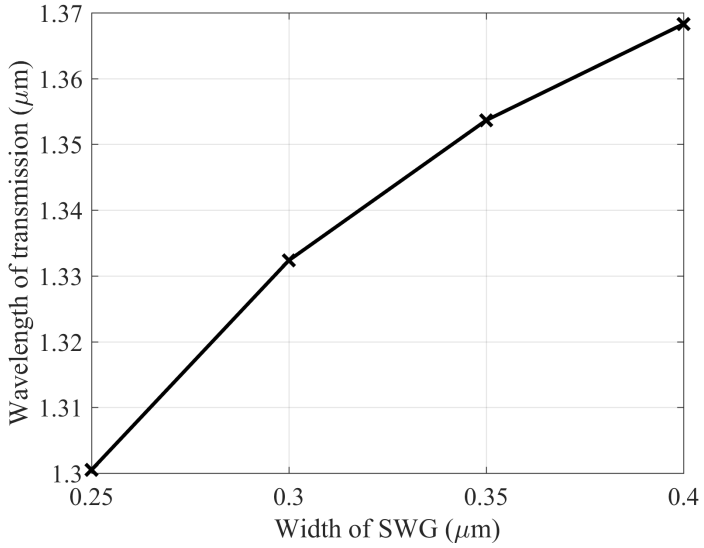

Figure 3.9: Transmission frequencies of contra-directional coupling for four SWGs $SWG_1 = 250nm$, $SWG_2 = 300nm$, $SWG_3 = 350nm$, $SWG_4 = 400nm$ and strip waveguide WG with width $280nm$

In this section, we have analytically described dependency of transmitted frequency of contra-directional coupler structure with strip waveguide and a sub-wavelength waveguide on the width of the SWG. Analogically, we could plot the same relationship for different widths of the central waveguide, different materials, or SWG pitch. This gives us all the tools we need to engineer our contra-directional coupler from wavelength point of view.

Mode shapes based on Marcatili method

To calculate field distribution in a rectangular waveguide using the Marcatili method, we split it into sectors, viz. Figure 2.9a. Taking advantage of symmetry of the structure, where all cladding sectors have the same $\epsilon_r 2$, we can calculate from $0 \rightarrow w/2$ for x and $0 \rightarrow h/2$ for y and mirror the rest along the axes.
As derived before, modes are calculated as superposition of two slab waveguide modes, TM and TE, each of them is either along x axis or y axis. Field in core, sector 1, can therefore be expressed as

$$U_1(x, y) = C_1 \cos(k_x x) \cos(k_y y) \tag{3.23}$$

where each cosine represents field distribution of 2D, TE or TM mode.
In upper cladding, sector 2, field distribution is given by

$$U_2(x,y) = C_2 \cos(k_x x) e^{-} k_{y2} y \tag{3.24}$$

where first cosine is representation of mode in x direction and the exponential is evanescent part of mode in y direction.
Analogically for sector 3, with swapped x and y.

$$U_3(x,y) = C_3 \cos(k_y y) e^{-} k_{x3} x \tag{3.25}$$

where k_y, k_{y2} and k_{x3} are propagation constants for y or x direction in sector 1, sctor 2 and sector 3 respectively. These constants can be calculated by plugging k_y or k_x from previous section back into dispersion relation.

$$k_{y2} = k_y \frac{\epsilon_r 2}{\epsilon_r 1} \tan\left(k_y \frac{h}{2}\right), k_{x3} = k_x \tan\left(k_x \frac{w}{2}\right) \tag{3.26}$$

For our case of rectangular waveguide of width $w = 280nm$ and $h = 220nm$ with core material $\epsilon_r 1 = 12.25$ and cladding $\epsilon_r 2 = 2.1025$ and working frequency $f = 230.6THz$ result is

$$k_{y2} = 11.574 \cdot 10^6, k_{x3} = 12.654 \cdot 10^6 \tag{3.27}$$

We can notice three constants C_1,C_2 and C_3. The first constant C_1 represents amplitude of the field for $x, y = 0$. We can set $C_1 = 1$ for now. C_2 and C_3 are calculated so boundary conditions on upper and right interfaced are fulfilled.
(3.23) has to be equal (3.24) for $y = h/2$ and $0 < x < w/2$. If we set $x = 0$ and $y = h/2$, we get following relation

$$U_1(x,y) = U_2(x,y) \tag{3.28}$$

$$C_1 \cos(k_x x)\cos(k_y y) = C_2 \cos(k_x x) e^{-} k_y y \tag{3.29}$$

$$\cos(k_y \frac{h}{2}) = C_2 e^{-} k_y \frac{h}{2} \tag{3.30}$$

$$C_2 = \frac{\cos(k_y \frac{h}{2})}{e^{-} k_y \frac{h}{2}} = 0.752 \tag{3.31}$$

Similarly for C_3, (3.23) has to be equal (3.25) for $0 < y < h/2$ and $x = w/2$. If we set $y = 0$ and $x = w/2$ then

$$U_1(x,y) = U_3(x,y) \tag{3.32}$$

$$C_1 \cos(k_x x)\cos(k_y y) = C_3 \cos(k_y y) e^{-} k_{x3} x \tag{3.33}$$

$$\cos(k_x \frac{w}{2}) = C_3 e^{-} k_x \frac{w}{2} \tag{3.34}$$

$$C_3 = \frac{\cos(k_x \frac{w}{2})}{e^{-} k_x \frac{w}{2}} = 2.291 \tag{3.35}$$

Now we can calculate the field profile for each sector and put them together to form one mode. Of course this method is limited to sectors in vertical or horizontal direction from core and we cannot solve the field profile in corner sections. Calculated mode profile is in

Field in SWG is generally very loosely confined, therefore to simulate its properties, we need to approximate it with very thin waveguide. For field profile calculations, we will replace the SWGs profile with rectangular waveguide of width merely $w = 170nm$ and height $h = 220nm$, its mode profile is in Figure

Before we move on, we need to normalize the modes to a power of 1W. To do that, we begin with electromagnetic field power formula, for electric and magnetic fields perpendicular.

$$P = \frac{\beta}{2\omega\mu_0} \iint |U(x,y)|^2 dxdy = 1 \tag{3.36}$$

where $U(x,y)$ is electroomagnetic field distribution, β is propagation constant and μ_0 permeability of free space. Therefore we need a coefficient K for which

$$K\frac{\beta}{2\omega\mu_0} \iint |U(x,y)|^2 dxdy = 1 \tag{3.37}$$

$$K \iint |U(x,y)|^2 dxdy = \frac{2\omega\mu_0}{\beta} \tag{3.38}$$

$$K = \frac{2\omega\mu_0}{\beta \iint |U(x,y)|^2 dxdy} \tag{3.39}$$

With field distributions power normalized, we can move on to calculating coupling coefficients.

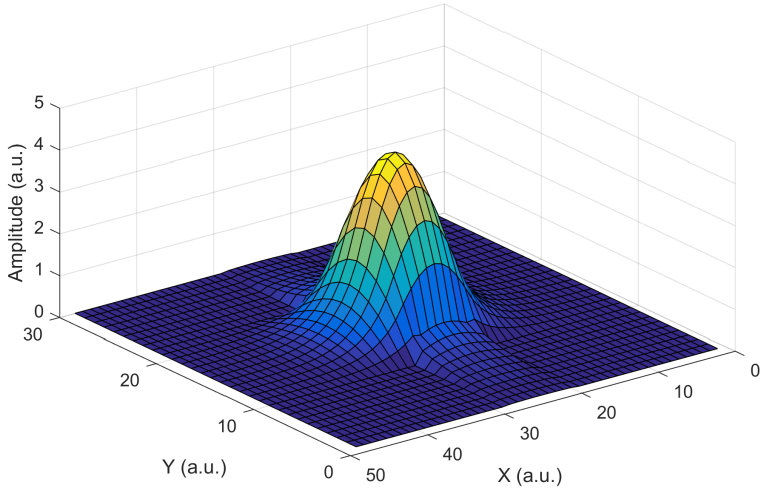

(a)

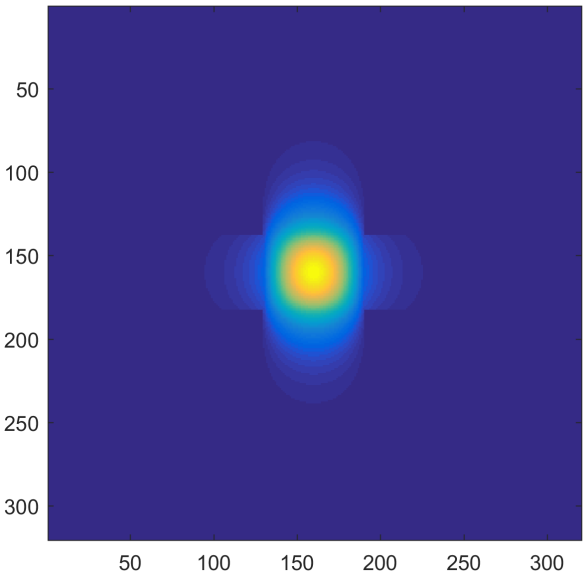

(b)

Figure 3.10: Calculated mode shape for rectangular waveguide with width $w = 280nm$ and height $h = 220nm$ using Marcatili method (a) surface plot (b) and 2D image

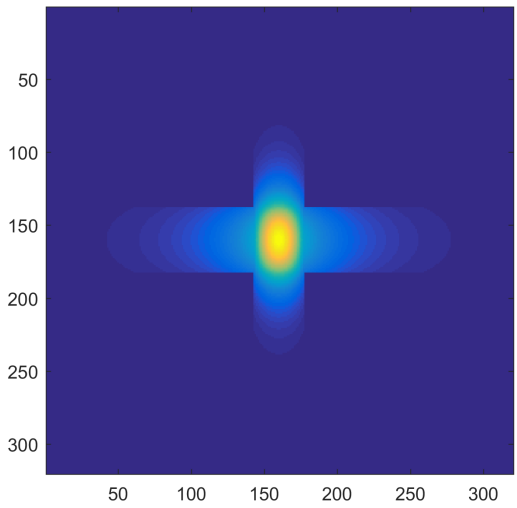

Figure 3.11: Calculated mode shape for rectangular waveguide with width $w = 170nm$ and height $h = 220nm$ using Marcatili method

Coupling coefficients κ of contra-directional coupler

Coupling coefficients represent field overlaps between modes. In this case, we are interested in mode interactions in the area of Bragg grating structure, which is the whole subwavelength waveguide cross section. We will calculate κ_{11} - coupling of center strip waveguide mode into it own, causing backreflection in the waveguide, $\kappa_{12} = \kappa_{21}^*$ coupling between strip waveguide and SWG and vice versa, and finally κ_{22} back reflections in SWG.

$$\kappa_{11} = \frac{\omega\epsilon_0}{4} \iint U_1(x,y) \cdot \delta\epsilon_r(x,y) U_1(x,y) dxdy \tag{3.40}$$

$$\kappa_{12} = \kappa_{21}^* = \frac{\omega\epsilon_0}{4} \iint U_1(x,y) \cdot \delta\epsilon_r(x,y) U_2(x,y) dxdy \tag{3.41}$$

$$\kappa_{22} = \frac{\omega\epsilon_0}{4} \iint U_2(x,y) \cdot \delta\epsilon_r(x,y) U_2(x,y) dxdy \tag{3.42}$$

where ω is angular frequency, $U_1(x,y)$,$U_2(x,y)$ are field profiles of waveguide and SWG respectively, and $\delta\epsilon_r(x,y)$ is Fourier expansion of perturbation function. We can notice that the perturbation function isn't a function of z, because it isn't the perturbation amplitude, but a Fourier coefficient.
We can calculate it is this way

$$\delta\epsilon_r(x,y,z) = \sum_{m=-1,1} \delta\epsilon_r(x,y) \cdot e^{-jm\frac{\pi}{\Lambda}z} \tag{3.43}$$

$$\delta\epsilon_r(x,y) = \frac{1}{\Lambda}\int_0^{\Lambda} \delta\epsilon_r(x,y,z) \cdot e^{jm\frac{\pi}{\Lambda})zdz} \tag{3.44}$$

$\delta\epsilon_r(x,y,z)$ is function of permittivity in all spatial directions. In our case,the perturbation is constant over x, y, because SWG is perceived as two homogeneous blocks with relative permittivity ϵ_{r1} and ϵ_{r2}. The relative permittivities are also constant in z direction for each half of the period. We will define new constant

$$\epsilon_{ravg} = \frac{\epsilon_{r1} + \epsilon_{r2}}{2} \tag{3.45}$$

so permittivity in the first half of period will be

$$\epsilon_{r\_first} = \epsilon_{r1} - \epsilon_{ravg} \tag{3.46}$$

and second half

$$\epsilon_{r\_second} = \epsilon_{r2} - \epsilon_{ravg} \tag{3.47}$$

Plugging these into (3.43), we get

$$\delta\epsilon_r(x,y) = \frac{1}{\Lambda}\int_0^{\Lambda} \delta\epsilon_r(x,y,z) \cdot e^{jm\frac{\pi}{\Lambda}}zdz = \frac{1}{\Lambda}\left[\int_0^{\Lambda/2} \epsilon_{r\_first} \cdot e^{jm\frac{\pi}{\Lambda}}zdz + \int_{\Lambda/2}^{\Lambda} \delta\epsilon_{r\_second} \cdot e^{jm\frac{\pi}{\Lambda}}szdz\right] \tag{3.48}$$

therefore

$$\Delta\epsilon_{+1} = j\frac{\epsilon_{r2} - \epsilon_{r1}}{\pi} = j\frac{12.25 - 2.1025}{\pi} = j3.23 \tag{3.49}$$

for $m = 1$ and previously specified materials. We can derive it for $m = -1$ as well and come up with similar result

$$\Delta\epsilon_{-1} = -j\frac{\epsilon_{r1} - \epsilon_{r2}}{\pi} = -j\frac{12.25 - 2.1025}{\pi} = -j3.23 \tag{3.50}$$

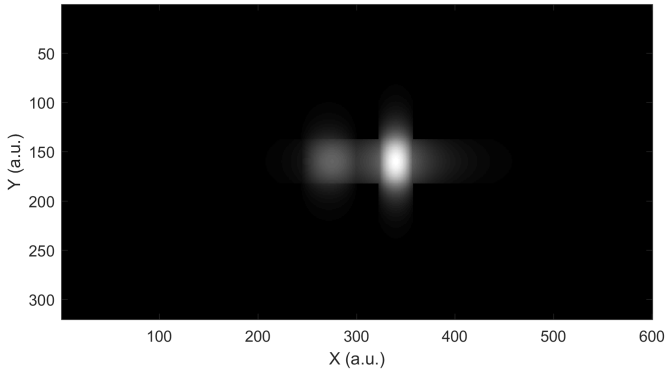

Figure 3.12: Two modes in close proximity for coupling coefficient calculation

Now we can calculate each coupling coefficient by integrating given mode shape over the SWG cross section. We place modes in Figure3.10b and Figure 3.11 in close proximity along the x axis, viz. Figure 3.12

Numerical values for each coupling coefficient, for $\epsilon_{r1} = 12.25$ $\epsilon_{r2} = 2.1025$, SWG dimensions $w = 300nm$, $h = 220nm$ and gap between the waveguides $g = 100nm$ are

$$\kappa_{11} = j774.6 \tag{3.51}$$

$$\kappa_{12} = \kappa_{21}^{*} = j18.872 \cdot 10^{3} \tag{3.52}$$

$$\kappa_{22} = j1.911 \cdot 10^{6} \tag{3.53}$$

We can see that κ_{11} is very small, that is because the evanescent field of strip waveguide isn't very strong in the SWG cross section, whereas κ_{22} is very big due to coupling of SWGs mode into itself. κ_{12} is around expected value.

Utilizing transfer matrix method to solve field amplitudes along z direction

To solve field at any place in space x, y, z, we can write it as a superposition of modes propagating in both waveguides. We will have modes propagating in the

forward direction, denoted with plus sign and in the backward direction, denoted with minus sign. The field equation is then written [1, 19, 20]

$$\mathbf{E}(x,y,z) = \left[A^+(z)e^{-j\overline{\beta_1}z} + A^-(z)e^{-j\overline{\beta_1}z}\right] U_1(x,y) + \left[B^+(z)e^{-j\overline{\beta_2}z} + B^-(z)e^{-j\overline{\beta_2}z}\right] U_2(x,y) \quad (3.54)$$

where $\overline{\beta_i}$ is generally complex propagation constant and is given by $\overline{\beta_i} = \beta_i - j\alpha$. We will consider only lossless waveguides, therefore α will be zero and real phase propagation constant β will remain. We can see the modes amplitudes A^i and B^i are function of z direction now. Differential equation for each mode are given [1, 19, 20]

$$\frac{dA^+}{dz} = -j\kappa_{11}A^-e^{j2\Delta\overline{\beta_1}z} - j\kappa_{12}B^-e^{j(\Delta\overline{\beta_1}+\Delta\overline{\beta_2})z} \quad (3.55)$$

$$\frac{dB^+}{dz} = -j\kappa_{12}A^-e^{j(\Delta\overline{\beta_1}+\Delta\overline{\beta_2})z} - j\kappa_{22}B^-e^{j2\Delta\overline{\beta_2}z} \quad (3.56)$$

$$\frac{dA^-}{dz} = j\kappa_{11}^*A^+e^{-j2\Delta\overline{\beta_1}z} + j\kappa_{12}^*B^+e^{-j(\Delta\overline{\beta_1}+\Delta\overline{\beta_2})z} \quad (3.57)$$

$$\frac{dB^-}{dz} = j\kappa_{12}^*A^+e^{-j(\Delta\overline{\beta_1}+\Delta\overline{\beta_2})z} + j\kappa_{22}^*B^+e^{-j2\Delta\overline{\beta_2}z} \quad (3.58)$$

where $\Delta\overline{\beta_i} = \beta_i - \frac{\pi}{\Lambda}$ is detuning parameter. The differential equations can be solved using transfer matrix method, where longitudinal relationship between z_1 and z_2 is givem by [1, 19, 20]

$$E(z_0) = C(z_0, z_1)E(z_1) \quad (3.59)$$

where

$$E(z) = \begin{bmatrix} E^+(z) \\ E^-(z) \end{bmatrix} = \begin{bmatrix} A^+(z) \\ B^+(z) \\ A^-(z) \\ B^-(z) \end{bmatrix} \quad (3.60)$$

and C is the transfer matrix. Its form can be analytically obtained from solution of (3.55) and was done in [19]

$$C(z0, z1) = e^{S_1(z_1 - z_0)} e^{S_2(z_1 - z_0)} \tag{3.61}$$

and the matrices S_1 and S_2 are given by [19]

$$S_1 = \begin{bmatrix} j\Delta\overline{\beta_1} & 0 & 0 & 0 \\ 0 & j\Delta\overline{\beta_2} & 0 & 0 \\ 0 & 0 & -j\Delta\overline{\beta_1} & 0 \\ 0 & 0 & 0 & -j\Delta\overline{\beta_2} \end{bmatrix} \tag{3.62}$$

and

$$S_2 = \begin{bmatrix} -j\Delta\overline{\beta_1} & 0 & -j\kappa_{11}e^{j2\Delta\overline{\beta_1}z} & -j\kappa_{12}e^{j(\Delta\overline{\beta_1}+\Delta\overline{\beta_2})z} \\ 0 & -j\Delta\overline{\beta_2} & -j\kappa_{12}e^{j(\Delta\overline{\beta_1}+\Delta\overline{\beta_2})z} & -j\kappa_{22}e^{j2\Delta\overline{\beta_2}z} \\ j\kappa_{11}^*e^{-j2\Delta\overline{\beta_1}z} & j\kappa_{12}^*e^{-j(\Delta\overline{\beta_1}+\Delta\overline{\beta_2})z} & j\Delta\overline{\beta_1} & 0 \\ j\kappa_{12}^*e^{-j(\Delta\overline{\beta_1}+\Delta\overline{\beta_2})z} & j\kappa_{22}^*e^{-j2\Delta\overline{\beta_2}z} & 0 & j\Delta\overline{\beta_2} \end{bmatrix} \tag{3.63}$$

(3.59) can be rewritten to [1, 19]

$$E(z_0) = \begin{bmatrix} E^+(z_0) \\ E^-(z_0) \end{bmatrix} \times E(z_1) = \begin{bmatrix} M^{++} & M^{+-} \\ M^{-+} & M^{--} \end{bmatrix} \begin{bmatrix} E^+(z_1) \\ E^-(z_1) \end{bmatrix} \tag{3.64}$$

where matrix M is total transfer matrix, in case of uniform grating $M = C$. If we are interested in through and drop channel, Equation (3.59) in this form isn't very useful, because it has inputs and outputs on both sides. We can rewrite the equation and separate inputs to right side and outputs to the left side. Matrix C will get transformed into the following form

$$\begin{bmatrix} A^+(z_1) \\ B^+(z_1) \\ A^-(z_0) \\ B^-(z_0) \end{bmatrix} = M' \begin{bmatrix} A^+(z_0) \\ B^+(z_0) \\ A^-(z_1) \\ B^-(z_1) \end{bmatrix} \tag{3.65}$$

where M' is transformed matrix M and defined from [1, 19]

$$M' = \begin{bmatrix} M^{++} - M^{+-}(M^{+-})^{-1}M^{-+} & M^{+-}(M^{--})^{-1} \\ -(M^{--})^{-1}M^{-+} & (M^{--})^{-1} \end{bmatrix} \tag{3.66}$$

Assuming input only from left side, $A^+(z_0)$ and $B^+(z_0)$, then $A^-(z_1)$ and $B^-(z_1)$ will be zero. Finally, we can write the relationship between inputs and outputs for uniform grating

$$\begin{bmatrix} A^+(z_1) \\ B^+(z_1) \\ A^-(z_0) \\ B^-(z_0) \end{bmatrix} = M' \begin{bmatrix} A^+(z_0) \\ B^+(z_0) \\ 0 \\ 0 \end{bmatrix} \tag{3.67}$$

To simulate apodized grating, we have to split the transfer matrix into partial matrices aong the z direction [20]

$$M_{total}(0, L) = M(L_{n-1}, L_n) \cdot M(L_{n-2}, L_{n-1})...M(L_0, L_1) \tag{3.68}$$

and each of the partial matrices will have its own calculated parameters, such as modified coupling coefficient. With the total matrix calculated, the process is then the same as for uniform grating.

Simulated spectral characteristics using coupled mode theory with transfer matrix method

With all waveguide parameters known from previous calculations, we can now numerically solve the transfer matrix from previous section. Again, we use the strip waveguide width of $w_{WG} = 0.28\mu m$ and four different SWGs with widths $w_{SWG1} = 0.25$, $w_{SWG2} = 0.3$, $w_{SWG3} = 0.35$, $w_{SWG4} = 0.4$ and period $\Lambda = 0.34\mu m$. At first, we will look at calculated spectral characteristics for uniform grating, viz. Figure 3.13

We can see peaks of transmission for each SWG width in agreement with previously calculated result, viz. Figure 3.9. Calculation for apodized grating was also performed

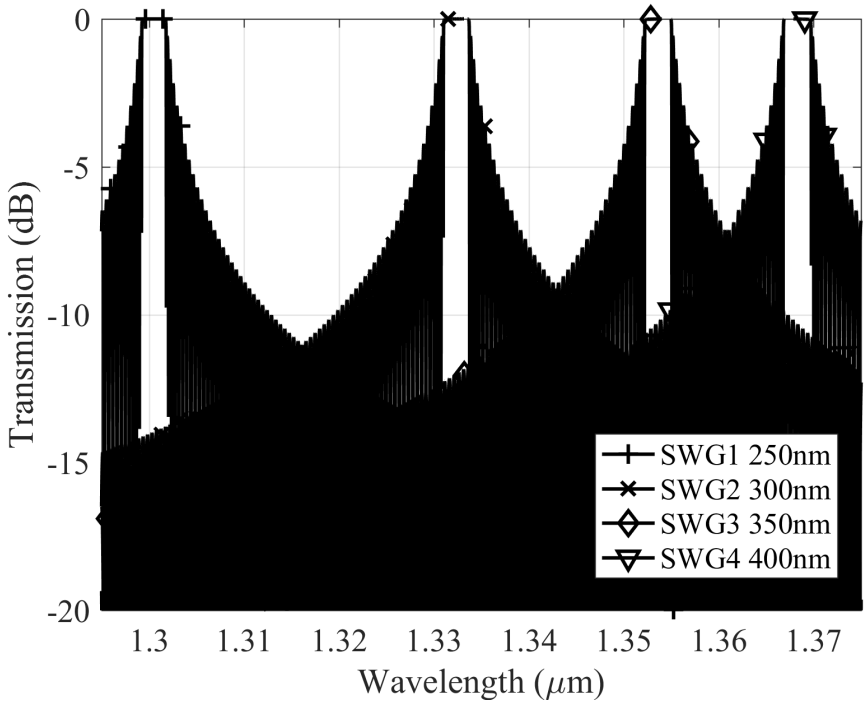

Figure 3.13: Calculated spectra for $w_{WG} = 0.28\mu m$, period $\Lambda = 0.34\mu m$ and $w_{SWG1} = 0.25\mu m$, $w_{SWG2} = 0.3\mu m$, $w_{SWG3} = 0.35\mu m$, $w_{SWG4} = 0.4\mu m$ using transfer matrix for uniform grating method

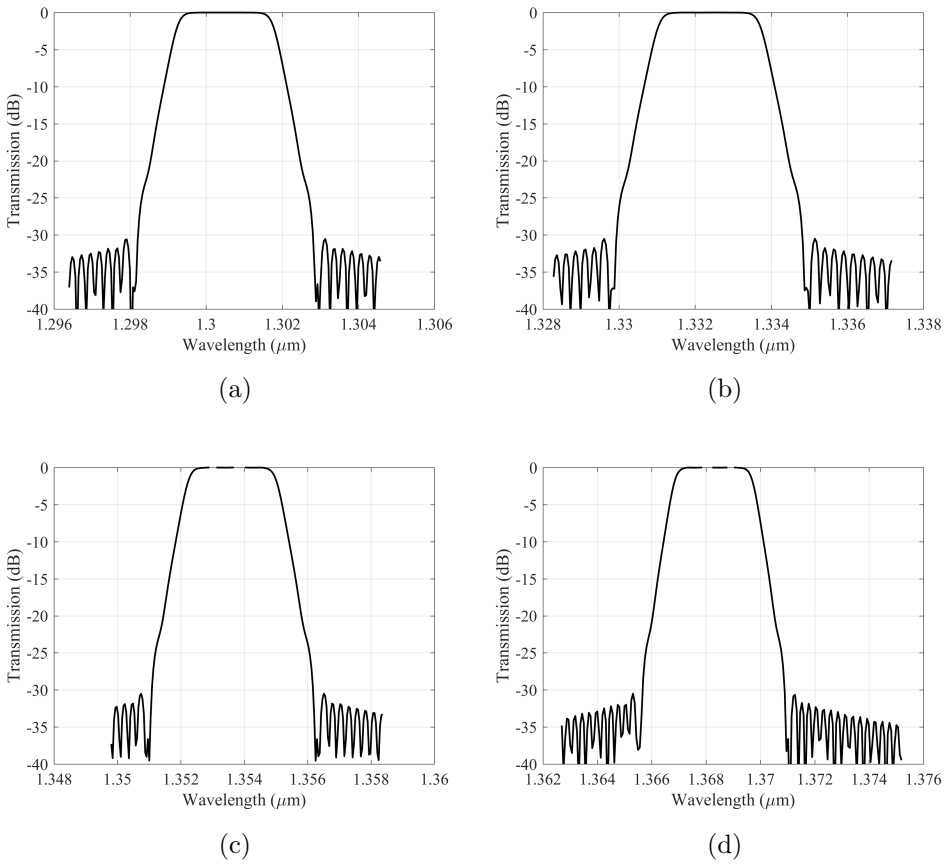

Figure 3.14: Calculated spectrum of contra-directional coupler with apodized grating for widths of SWG (a) $w_{SWG1} = 0.25\mu m$ (b) $w_{SWG2} = 0.3\mu m$ (c) $w_{SWG3} = 0.35\mu m$ (d) $w_{SWG4} = 0.4\mu m$

Chapter 4

Simulation Results

4.0.1 Simulation Setup

To verify designed structure, analytic approximation and various numerical simulations were performed. Derived analytic approximation using Coupled Mode Theory with transfer matrix method was calculated in Matlab and most numerical simulations in this work were done in Lumerical MODE Solutions, Lumerical FDTD Solutions, and Lumerical Interconnect. Lastly, the design was also verified in IMT Photonic Bands using a different method of obtaining band diagrams. MODE Solutions is design environment for analysis and optimization of various passive optical components, such as integrated optics, tapers, couplers and resonators, Bragg gratings and more. It features modal analysis for investigation of spatial fields, modal frequency analysis, confinement factor etc., Bidirectional Eigenmode Expansion (EME) propagation ideal for long periodic structures and large propagation length and variational FDTD (varFDTD) for very fast analysis of structures with planar waveguide geometries[21].

Finite-difference time-domain (FDTD) method of simulation is very accurate and versatile technique for simulating various problems in nanophotonics. However, it can be very computationally exhaustive when large amount calculation points are used. This mainly is a problem of 3D FDTD, which makes it difficult to simulate large structures. The varFDTD provides comparable accuracy, but with speeds only slightly bigger than 2D FDTD. The method involves collapsing 3D

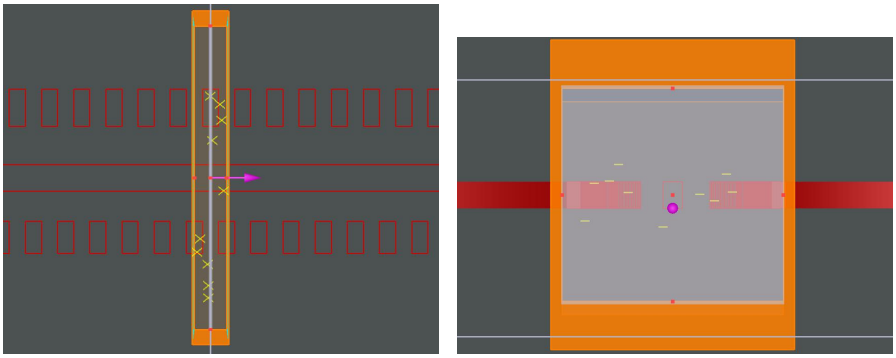

(a) (b)

Figure 4.1: (a) XY and (b) YZ views for bandstructure simulation in Lumerical FDTD

structures into 2D, converting the third dimension into dispersive materials that account for classic material properties as well as waveguide dispersion [21]. As opposed to Lumerical Suite, IMT Photonic bands use simulations in frequency domain.

Lumerical FDTD bandstructure simulations setup

To calculate bandstructure simulations in Lumerical FDTD, we set simulation region length in z direction to the length of one period of SWG and boundary conditions set to be periodic, basically copying resulting fields at the end back to the beginning and applying phase correction at the same time. XY and YZ views exported from Lumerical FDTD are shown in Figure 4.1. Mesh is selected to be dividing the simulation region in z direction into 16 equal lengths to make sure that period is calculated correctly. In x and y direction, mesh is set to automatically accommodate the structure dimensions. Simulation time is set 2000ps for spectral peaks to develop correctly and minimize noise. There are 10 time domain point monitors scattered in the simulation region, for any given k, Bloch, vector, each of them is evaluated by a script and result converted to frequency by Fourier transformation. Sweeping the Bloch vectors will result in bandstructure plot.

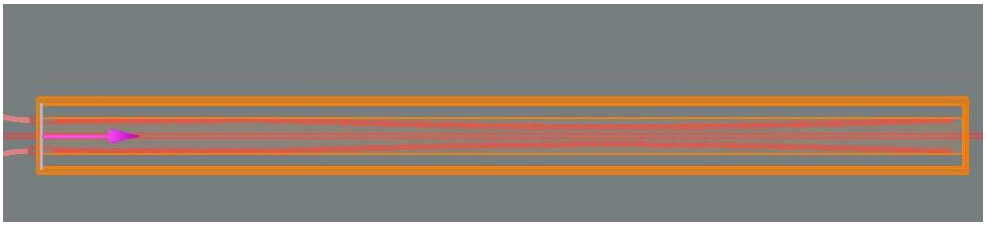

Figure 4.2: XY view of spectral 3D FDTD Simulation

Spectral simulation with Lumerical FDTD and Mode

Simulating long structures by FDTD simulation is very time inefficient, therefore we try to utilize the bandstructure simulation technique as often as we can. For simulating spectral properties, there are not many other choices left. Especially, if we want to simulate non-uniform grating, such as apodized or chirped. To understand spectral properties, we utilized mainly Mode Solutions 2.5D varFDTD. With speeds close to 2D FDTD, it gives better results. However, it will be shown later that we cannot rely on the frequency results, however, the overall spectral shape is still useful. Thus, we use 2.5D to show spectral shape properties with high-resolution mesh and 1300 periods, and 3D FDTD to compare the peak reflected wavelengths with bandstructure simulation. However, even with low amount of periods, we can not afford very high-resolution mesh. It will be shown that reflected wavelength and spectral shape is strongly dependent on mesh size. For this reason, bandstructure simulation is regarded as the one closest to the real characteristics of proposed structure. XY image from simulation of our apodized contra-directional coupler segment is in Figure 4.2

4.0.2 Simulation Results and Optimization of parameters

When analyzing and optimizing presented structure, we have to consider the basic condition for contra directional coupling (2.165)

$$\beta_1 + \beta_2 = \frac{2\pi}{\Lambda} \tag{4.1}$$

and Bragg reflection condition (2.164)

$$\beta_{reflected} = \frac{\pi}{\Lambda} \tag{4.2}$$

To achieve good spectral results we need to keep propagation constants β_1 and β_2 dissimilar enough so unwanted backreflection (4.2) is not satisfied in wavelength band satisfying (4.1). The propagation constant of the strip waveguide is adjusted by changing the width, the propagation constant of SWG can be adjusted either by modulating a duty cycle of segments or similarly to a regular waveguide by adjusting the width of segments. In this design, the latter was chosen for simplicity and necessity to follow fabrication design rules. Finally, we can adjust the pitch of SWG segments to control Bragg reflected wavelength. It will be shown, that pitch and width of the center strip waveguide both have very big impact on the wavelength of reflected mode, therefore we use them to set the overall channel wavelength band (in this case around 1300nm for O-band). The width of SWG has less pronounced effect so we can utilize it to tune the final wavelength for each channel.

In this section, simulation results for the design parameters are shown. Simulation is done with 3D FDTD by bandstructure simulation method. This kind of simulation allows us to see excited modes of each subwavelength waveguide and strip waveguide.

In following graphs of this chapter, we will see propagation constants of strip waveguide plotted against propagation constants of subwavelength waveguides. From the nature of SWGs and all periodic structures, diffraction graphs will mirror along the irreducible Brillouin zones. Even though simple strip waveguide isn't a periodic structure by itself, we introduce artificial periodicity by limiting simulation length to one period of SWG. We can take advantage of this mirroring for evaluation of the results by plotting diffraction graphs for $0 < k\frac{a}{2\pi} < 0.5$ and determining the reflected frequency by observing the crossings of diffraction lines of SWG and mirrored waveguide plots. When the lines cross they will have following propagation constants

$$k_{norm\_SWG} = q \cdot k\frac{a}{2\pi}, 0 < q < 0.5 \tag{4.3}$$

$$k_{norm\_WG\_mirred} = 0.5\frac{a}{2\pi} + \left(0.5\frac{a}{2\pi} - q \cdot k\frac{a}{2\pi}\right) = \frac{a}{2\pi} - q \cdot k\frac{a}{2\pi} \tag{4.4}$$

if we add these normalized propagation constants together

$$k_{norm} = k_{norm\_SWG} + k_{norm\_WG\_mirred} = q \cdot k\frac{a}{2\pi} + \frac{a}{2\pi} - q \cdot k\frac{a}{2\pi} = \frac{a}{2\pi} \qquad (4.5)$$

and the contra-directional coupling condition (4.1) is satisfied. This principle will be utilized in all bandstructure simulations.

Period of subwavelength waveguide

Period modulation is a standard method to control the wavelength of contra-directional coupler [1]. This approach is well suited for large scale wavelength tuning, however, it could prove difficult to fabricate minute changes in pitch to ensure a good accuracy of each channel center wavelength. In this simulation, we investigated the effect of period modulation on central reflected wavelength. For this simulation, bandstructure method was used. In Figure 4.3a, we can see the resulting dispersion curves. For each simulated period, there are two SWGs and one strip waveguide with widths $w_{SWG1} = 0.3\mu m$, $w_{SWG2} = 0.4\mu m$ and $w_{WG} = 0.28\mu m$. Each such dispersion curve triplet is labeled with a different symbol in the graph. From the nature of the simulation, we can see the shift of first Brillouin zone due to the change in period. To better show the trend, points, where the contra-directional condition is satisfied, are plotted in Figure 4.3b. Both SWGs show similar and expected rising trend of center reflected wavelength with the period. To assess the magnitude of change, both curves are linearly fitted, and the ratio of change is found to be 2.043 for SWG_1 and 1.987 for SWG_2. This means, that if we change period by $1nm$, the central wavelength will shift by $2nm$, therefore to change the channel of the LAN-WDM demultiplexer to one higher, we would need change period of SWG by approximately $2.25nm$, which could prove difficult to fabricate. For this reason, we decided to keep all periods fixed at $\Lambda = 0.34\mu m$, where we can fit all eight LAN-WDM channels. Furthermore, keeping period constant, we can mutually shift the two SWGs by $\Lambda/2$ to minimize their interaction and therefore reduce crosstalk. Lastly, there is also one practical advantage, we can set simulation mesh to precisely match the SWGs material boundary at any point in the structure, to maximize the

calculated precision.

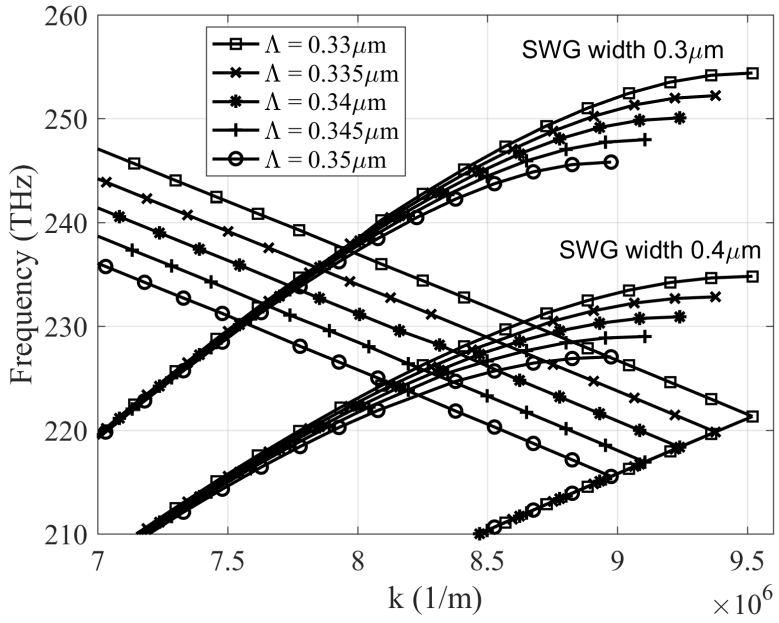

(a)

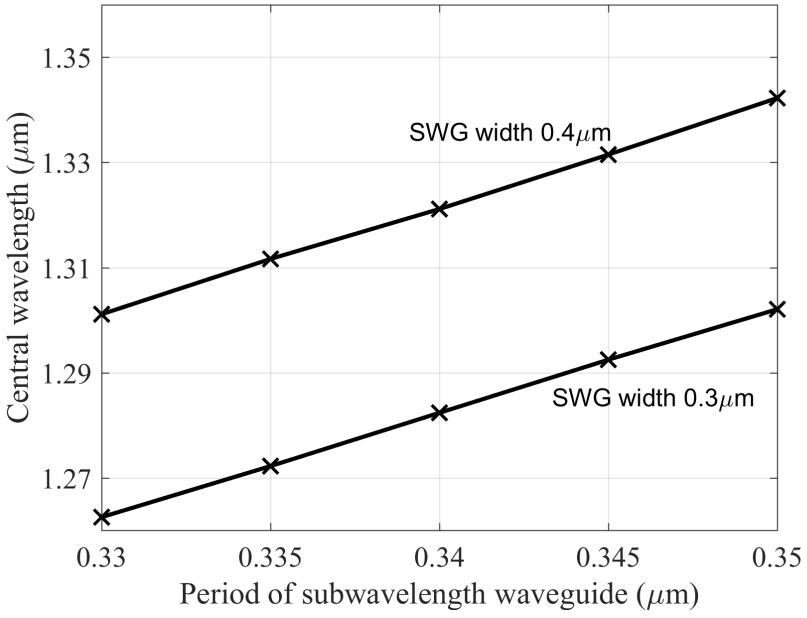

(b)

Figure 4.3: Simulation of two SWGs with width $w_{SWG1} = 0.3\mu m$, $w_{SWG2} = 0.4\mu m$ and strip waveguide with width $w_{WG} = 0.28\mu m$ for periods of SWG $0.33\mu m$, $0.335\mu m$, $0.34\mu m$, $0.345\mu m$ and $0.35\mu m$ plotted as diffraction curves (a) and relation between period of SWG and reflected wavelength (b)

Width of center strip waveguide

By adjusting the width of center strip waveguide, we change its propagation constant and therefore reflected frequency. To get the propagation constant in a usable area, we use relatively narrow strip waveguide, around $280nm$, which has confinement factor of are 85% (calculated by Lumerical FDE Solver), therefore, change of the propagation constant with the change of width will be significant. To learn more about the trend, bandstructure calculation for 5 different widths of the center strip waveguide, $w_{WG1} = 0.25\mu m$, $w_{WG2} = 0.265\mu m$, $w_{WG3} = 0.28\mu m$, $w_{WG4} = 0.295\mu m$, $w_{WG5} = 0.31\mu m$, was simulated. Widths of SWGs are $w_{SWG1} = 0.3\mu m$, $w_{SWG2} = 0.4\mu m$ and their period is $\Lambda = 0.34\mu m$. Simulated dispersion curves are in the Figure 4.4a. We can see propagation constant rises with increased width of strip waveguide, which is to be expected since the light is getting more and more confined in waveguide core which has a higher index of refraction than the cladding. For strip waveguide WG1 and SWG2, we notice that their propagation constants are almost matched, which causes two problems, reflected wavelength is getting close to the bandgap of SWG, limiting the bandwidth due to its back reflection. The second problem could arise, if strip waveguide and SWG get phase matched, the structure would start to behave like a directional, not contra-directional, coupler. Therefore, we need to be aware of these parameters when designing our contra-directional coupler and keep the waveguides sufficiently asymmetric. In Figure 4.4b relationship between the width of strip waveguide width and reflected wavelength. For both SWG1 and SWG2 the trend seems fairly linear with a slightly lower rate for SWG2. Fitted linear curve gives us a rate of change for SWG1 0.9618 and SWG2 0.7253, thus change in width of strip waveguide causes a shift of reflected wavelength by $0.96nm$ in SWG1 and $0.72nm$ in SWG2. While this rate of change is smaller than that of changing period, it is still fairly high and it would be inconvenient to try and match it for both SWGs, therefore we keep the width of strip waveguide constant at $w_{WG} = 0.28\mu m$.

Width of subwavelength waveguide

Similarly to the strip waveguide, changing the width of subwavelength waveguide affects propagation constant. In the previous chapter, we showed that it can be explained as a change in propagation constant of the high-index part of SWG. Bandstructure simulation was utilized again to get insight on the trend. Simulation was done for SWG widths $w_{SWG1} = 0.25\mu m$, $w_{SWG2} = 0.3\mu m$, $w_{SWG3} = 0.35\mu m$, $w_{SWG4} = 0.4\mu m$, period constant $\Lambda = 0.34\mu m$ and strip waveguide $w_{WG} = 0.28\mu m$. Resulting dispersion curves are in Figure 4.5. Given the parameters of strip waveguide and SWGs, we can see good asymmetricity for SWG width from $0.3\mu m$ to $0.4\mu m$, corresponding to the whole range of 8 channel LAN-WDM. Corresponding reflected wavelength as a function of SWG width is plotted in Figure 4.3b. The resulting trend seems to be linear for SWG width more than $0.3\mu m$. Fitting linearly, we get a coefficient of 0.322, therefore change in width of SWG by $1nm$ will cause a shift in reflected wavelength by $0.322nm$. From all the parameters simulated before, this rate is by far the smallest, and thus we utilize it to precisely set up LAN-WDM channels, with more immunity to fabrication error. Adjusting subwavelength width is preferred the method to set the reflected wavelength of proposed contra-directional coupler.

With all the design parameters described, we can now plot dispersion curves for all LAN-WDM channels, viz. Figure 4.6 For strip waveguide width set $w_{WG} = 0.28\mu m$, SWG period constant across all channels $\Lambda = 0.34\mu m$ we can calculate all the widths of SWGs listed in Table 4.1, where λ and f are wavelength and frequency of each channel respectively, and w_{SWG} is corresponding width of SWG.

Comparison of analytical and numerical results

To assess the accuracy of our proposed analytical solution, we compare the calculated and simulated central wavelengths as a function of SWG width, viz. Figure 4.7. We can observe, that calculation gives us higher values and slightly different trend. This is attributed to the approximation of subwavelength waveguides propagation constant (3.20). In Figure 4.8, difference of both results is plotted.

Chan.	1	2	3	4	5	6	7	8
$\lambda(\mu m)$	1.2822	1.2866	1.2911	1.2955	1.3045	1.3091	1.3137	1.3183
$f(THz)$	233.8	233	232.3	231.4	229.8	229	228.2	227.4
$w_{SWG}(\mu m)$	0.2995	0.3128	0.3251	0.3371	0.3601	0.3712	0.3821	0.3927

Table 4.1: Simulated widths of SWG corresponding to LAN-WDM grid, viz. Table 2.1

We can see deviation varying from $32nm$ to $55nm$. Therefore, to use this analytical solution for actual demultiplexer design, we would need to find an even better approximation of subwavelength waveguide propagation properties.

In real world we have to think about fabrication processes and tolerances. While adjusting the width of waveguides in simulation looks as a preferable approach, the tolerances are considerable higher than those of pitch between tho waveguides. Thus, the advantages of low sensitivity to change of the width of the SWG might be reduced by higher fabrication error.

Spectral simulations of contra-directional coupler

For spectral simulations, we employed both 3D ad 2.5D FDTD. To verify results from previous bandstructure simulation, we tried to use more accurate, however very computational power demanding 3D FDTD. To keep simulation time reasonable, we had to keep mesh very rough even when we are only simulating each segment containing one strip waveguide and two SWGs. Therefore four separate simulations were made to obtain the full spectrum. Parameters obtained from previous bandstructure simulations were used to compare the spectral peaks wavelengths. Some difference is to be expected given the discrepancy in mesh accuracy, as well as poor spectral shape. Result of rough mesh 3D FDTD simulations of all 4 segments is in Figure 4.9.

As expected, we can see poor spectral shape and central wavelengths deviating from expected results for SWGs widths given by Table 4.1. Deviation

Chan.	1	2	3	4	5	6	7	8
$\Delta\lambda(nm)$	-6.7	-5.3	-6.5	-5	-7	-5.4	-6.6	-4.6

Table 4.2: Deviation of 3D FDTD spectral simulation with coarse mesh from bandstructure simulation.

of central wavelengths from expected value is written in Table 4.2 and plotted in Figure 4.10, where $\Delta\lambda = \lambda_{expected} - \lambda_{simulated}$. The simulated results show consistently lower center wavelength, oscillating around $\Delta\lambda = 6nm$.

To verify, the discrepancy is indeed result of coarse mesh, we made two other simulations for $L0$ and $L2$, with medium and fine mesh. Number of simulated periods had to be lowered with each mesh definition increment to keep simulation times reasonable. For coarse mesh $N = 1200$ periods were used, for medium mesh $N = 450$, and fine mesh $N = 200$. Due to the varying number of periods, spectral shape is different. Result of these simulations is in Figure 4.11

and deviation $\Delta\lambda$ plotted again in Figure 4.12

We can see the clear trend of decreasing deviation with lower mesh size, which gives us confidence in previous bandstructure simulation, where the mesh is even finer than the finest in the spectral simulation. However, it is very hard to assess real spectral performance without simulating all $N = 1300$ periods while having fine mesh. For this reason, we also utilized Lumerical's Mode 2.5D varFDTD.
3D FDTD is obviously superior to the 2.5D varFDTD in accuracy and would be the preferred method of calculation. However, in our case, to use the 3D FDTD, we have to choose between number of periods, therefore length of the structure, or simulation precision otherwise simulation time and requirements would not be manageable. Thus, we concluded, that even though 2.5D varFDTD is inferior to 3D FDTD in all parameters, we can simulate whole length of the structure with ultra-fine mesh and the result will be better representation of real spectral behavior.
To save computational time, the 2.D varFDTD has to make many approximations of the 3D structure into 2D space. In our simulation, we noticed bigger calculated

propagation constants, therefore resulted central wavelengths were higher than those by 3D FDTD bandstructure and spectral simulations. To account for that, period of subwavelength grating was lowered from $\Lambda_{3D} = 0.34\mu m$ to $\Lambda_{2.5D} = 0.315\mu m$. Thus, this simulation is mainly verification of spectral shape and not of the absolute values of central wavelengths. Simulated spectrum is shown in Figure 4.13. We can see spectral characteristics with flat top and insertion loss less than 1dB and very good adjacent channel suppression of more than 30dB. This simulation does not take into account possible losses in MZI separating the channels into two groups.

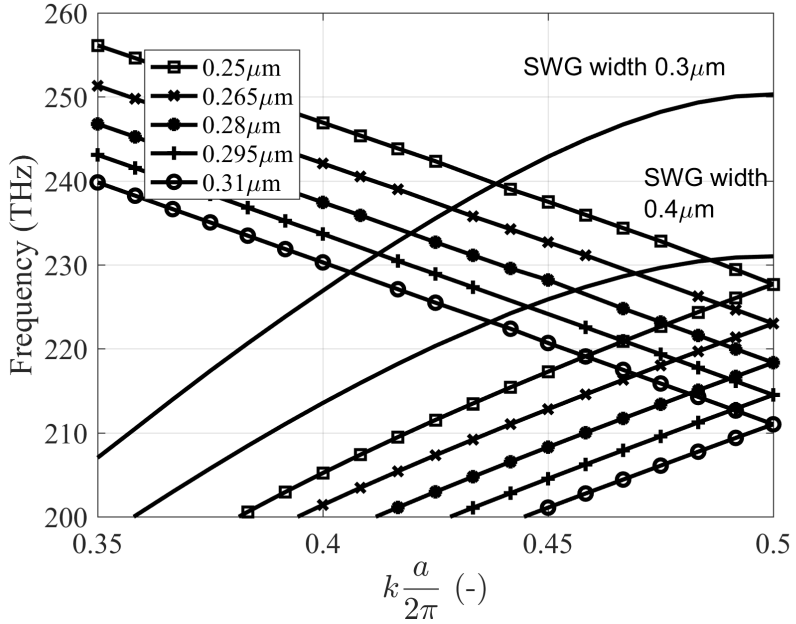

(a)

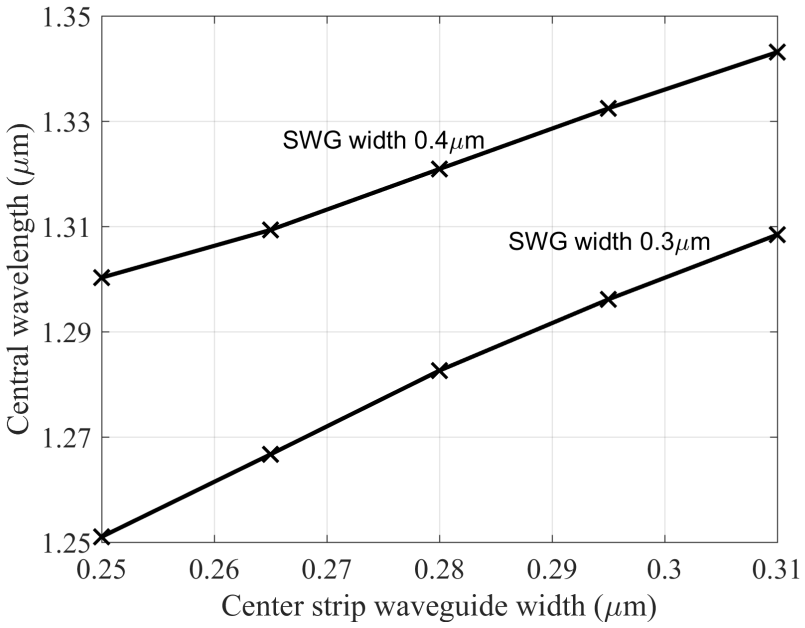

(b)

Figure 4.4: Simulation of two SWGs with width $w_{SWG1} = 0.3\mu m$, $w_{SWG2} = 0.4\mu m$ and period $\Lambda = 0.34\mu m$ and strip waveguide with varying widths $w_{WG1} = 0.25\mu m$, $w_{WG2} = 0.265\mu m$, $w_{WG3} = 0.28\mu m$, $w_{WG4} = 0.295\mu m$, $w_{WG5} = 0.31\mu m$ plotted as diffraction curves (a) and relationship of the width with reflected wavelength (b)

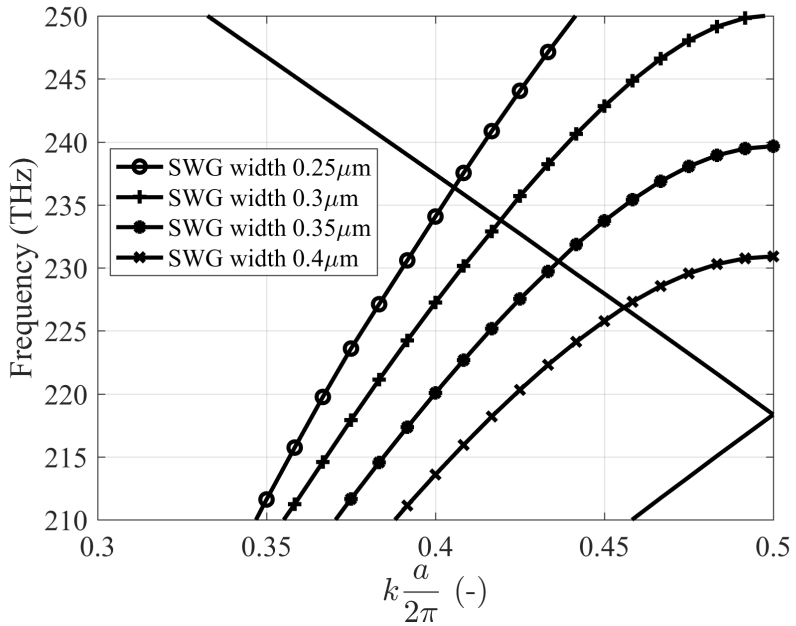

(a)

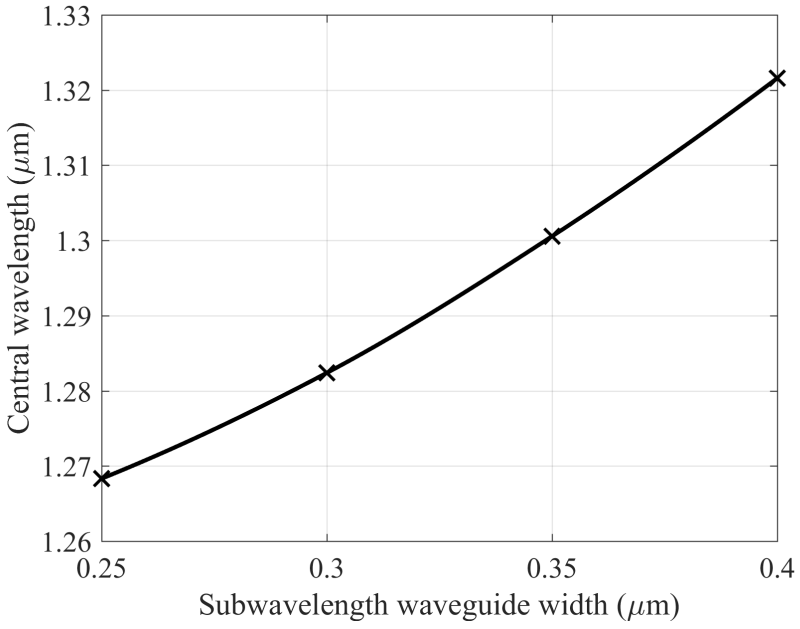

(b)

Figure 4.5: Simulation for varying widths of SWGs $w_{SWG1} = 0.25\mu m$, $w_{SWG2} = 0.3\mu m$, $w_{SWG3} = 0.35\mu m$, $w_{SWG4} = 0.40\mu m$, with constant period $\Lambda = 0.34\mu m$ and strip waveguide width $w_{WG1} = 0.28\mu m$ plotted as diffraction curves (a) and relationship of the SWG width with reflected wavelength (b)

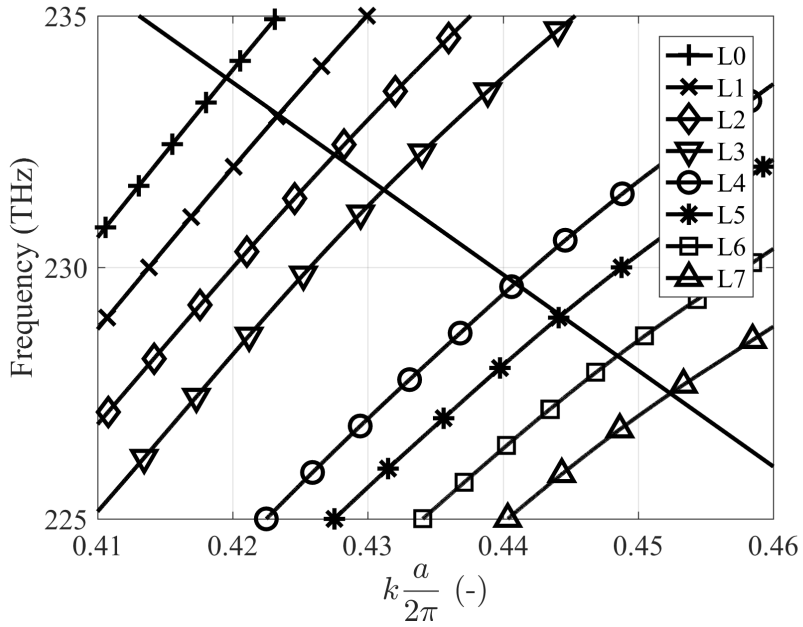

Figure 4.6: Dispersion curves for 8 SWGs and strip waveguide corresponding to 8 channels of LAN-WDM, viz. Table 2.1

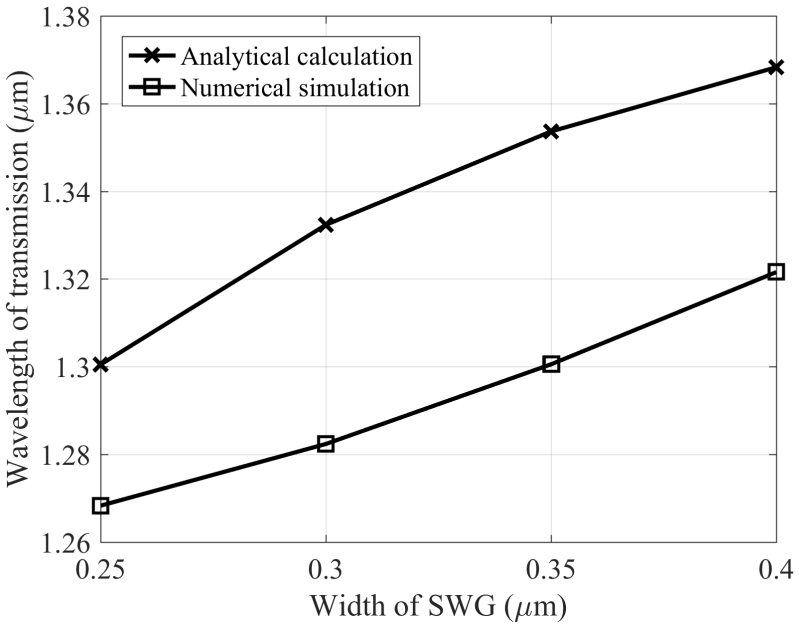

Figure 4.7: Central wavelength as function of SWG width for analytical calculation and numerical simulation

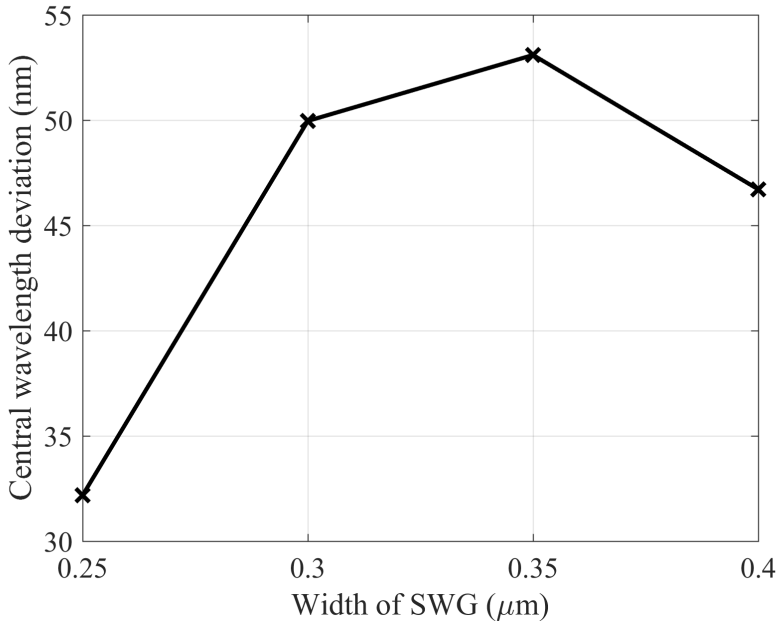

Figure 4.8: Difference in central wavelengths of calculated and simulated results

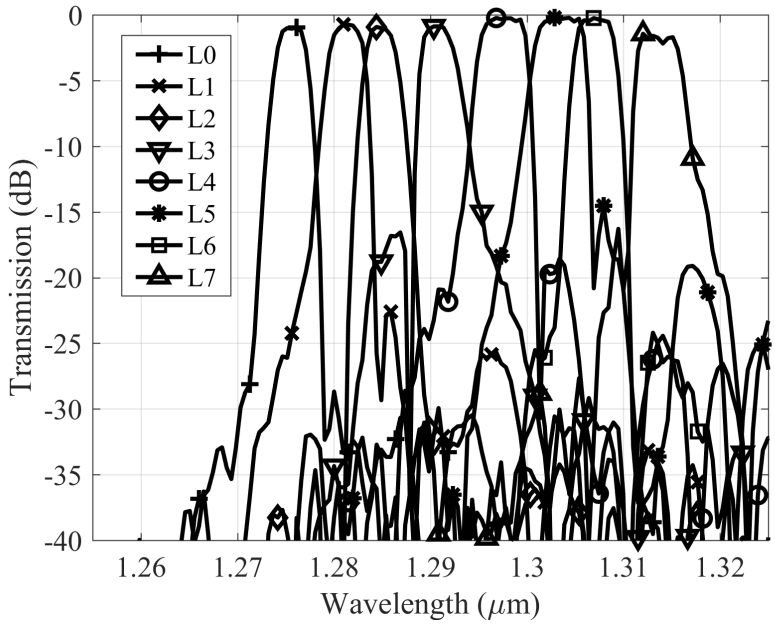

Figure 4.9: Spectrum simulation of 8 LAN-WDM channels, viz. Table 4.1, by 3D FDTD with rough mesh for $N = 1200$ periods

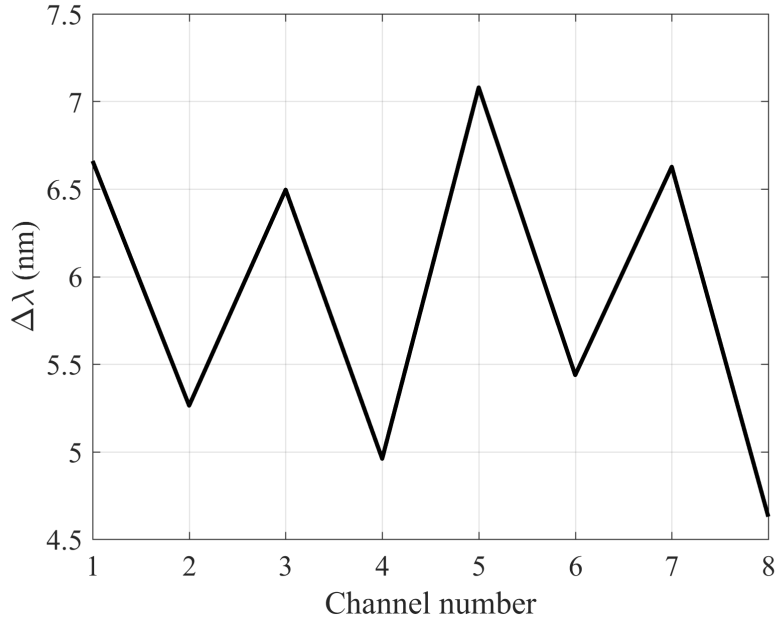

Figure 4.10: Deviation of central wavelength from expected values given by Table 4.1

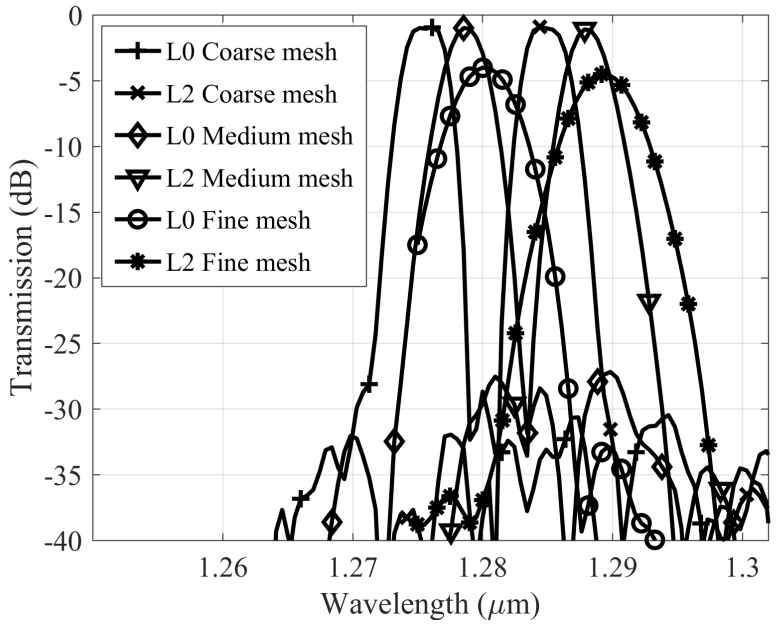

Figure 4.11: Comparison of simulations with difference sizes of mesh, from very coarse to fine, for L0 and L2, different shape is given by number of periods simulated, for coarse mesh $N = 1200$ periods, medium mesh $N = 450$, and fine mesh $N = 200$

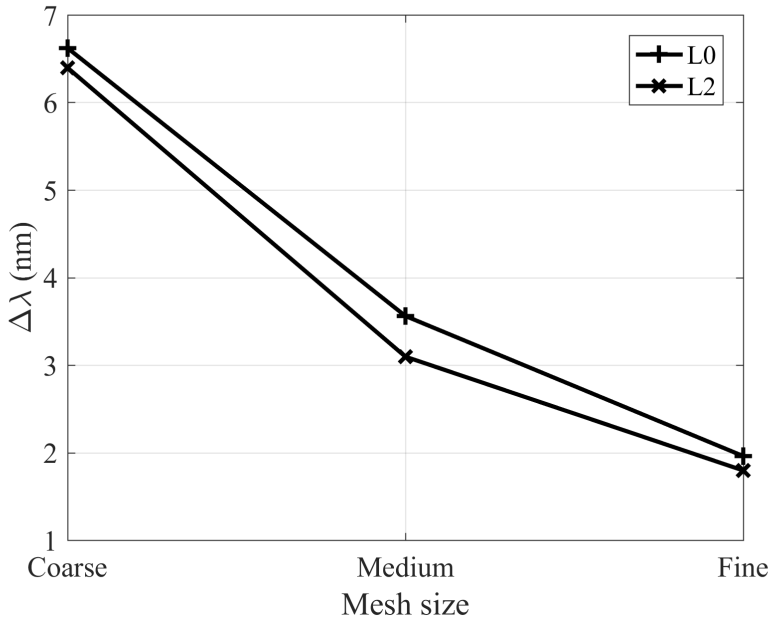

Figure 4.12: Deviation of central wavelength from expected result for three different simulation mesh size

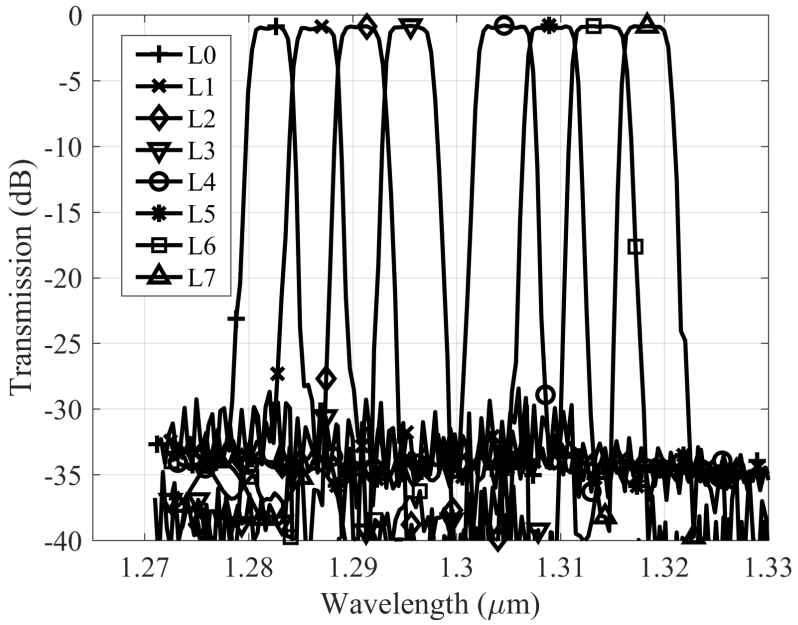

Figure 4.13: Spectrum simulated in Lumerical Mode 2.5D var FDTD

Chapter 5

Conclusion

In this thesis, novel 8-channel demultiplexer based on grating-assisted couplers was investigated. Consisting of strip waveguide and a subwavelength waveguide, proposed structure is an evolution of currently used structures, such as in [1]. The motivation for this work was given by the lack of integrated solutions for new metropolitan network system LAN-WDM, being a compromise between previously extensively used CWDM and DVDM. Therefore, such solution is provided with theoretical analysis and numerical calculations.

Analytical approximation, utilizing Marcatili's method for waveguide properties definition and coupled mode theory used for calculation of spectral characteristics, is described. Novel approximation technique of subwavelength waveguide effective index was used to explain the principle of operation. From this analysis, we can obtain relationship between center wavelength of demultiplexed signal and various design parameters, such as center strip waveguide as well as SWG width and thickness, materials, or SWG period. For obtained wavelengths, we can plot the spectrum of uniform or apodized grating. Structure with four different widths of subwavelength waveguides was calculated, for period $\Lambda = 0.34\mu m$ and width of the strip waveguide $w_{WG} = 0.28\mu m$. Resulted calculated central wavelengths of demultiplexed signals were $\lambda_1 = 1.301\mu m$, $\lambda_2 = 1.332\mu m$,$\lambda_3 = 1.354\mu m$ and $\lambda_4 = 1.368\mu m$ for SWG widths $w_{SWG1} = 0.25\mu m$, $w_{SWG2} = 0.30\mu m$, $w_{SWG3} = 0.35\mu m$ and $w_{SWG4} = 0.40\mu m$ respectively. Numerical bandstructure simulation in Lumerical FDTD was performed to precisely assess effect of period,

and waveguide properties on center wavelength. It was shown, that change of $1nm$ in period results in around $2nm$ change in center wavelength, for change in width of the strip waveguide it was $0.7nm$ and $1nm$ for $w_{SWG1} = 0.3\mu m$, $w_{SWG1} = 0.4\mu m$ respectively and $0.33nm$ per $1nm$ change in width of SWG. The period has, therefore, the biggest impact, followed by the width of the strip waveguide and the least effect has the width of SWG. Consequently, following approach to design was taken - using period and width of the strip waveguide to set adequate band (in our case wavelength around 1300nm), to assure good asymmetricity and then use the SWG width to precisely set each channels' demultiplexing wavelength. Final parameters of the structure are - width of strip waveguide $w_{WG} = 0.28\mu m$, period of subwavelelngth waveguide $\Lambda = 0.34\mu m$, and SWG with varying widths $0.3\mu m < w_{SWG} < 0.4\mu m$. After obtaining precise parameters, a spectral simulation was done to verify previous results and show spectra properties. Due to the difficulty of simulation, 3D FDTD was only used to verify predictions of bandstructure simulation, however, the computational complexity limited the accuracy. The dependency of simulated central wavelength on mesh size was demonstrated, when simulation with coarse mesh showed a deviation of around $6nm$, lowered to around $3.5nm$ with medium sized mesh and finally to about $2nm$ for the fine mesh. Since the previous bandstructure simulation had even finer mesh, we can have good confidence in those results. To show the spectral shape of each channel, 2.5D varFDTD was utilized, allowing for fine mesh and big simulation region in exchange of absolute accuracy. The period had to be modified to fit within the bandwidth of LAN-WDM, however, in this simulation, we are interested in the shape of the spectrum, not its absolute value in terms of wavelength. Resulting spectrum shows insertion loss of less than 1 dB and great suppression of adjacent channel of more than 30 dB.

Work in this thesis can be used for understanding and design of a new type of integrated contra-directional grating assisted gratings, showing evidence of great tunability and spectral properties.

Bibliography

[1] W. Shi, X. Wang, C. Lin, H. Yun, Y. Liu, T. Baehr-Jones, M. Hochberg, N. A. F. Jaeger, and L. Chrostowski. "Silicon photonic grating-assisted, contra-directional couplers". In: *Opt. Express* 21.3 (Feb. 2013), pp. 3633–3650.

[2] T. Paatzsch, I. Smaglinski, and S. Krüger. "Compact Optical Multiplexers for LAN WDM". In: *IEEE 802.3ba Task Force* (July 2008).

[3] G. Agrawal. *Fiber-optic communication systems*. Wiley series in microwave and optical engineering v. 1. Wiley-Interscience, 2002.

[4] B. Mukherjee. *Optical WDM Networks*. Optical Network v. 1. Springer US, 2006.

[5] L. Gasca. *From O to L: The Future of Optical-Wavelength Bands*. 2008. URL: `http://www.bbcmag.com/2008issues/june08/BBP_June08_OtoL.pdf`.

[6] International Telecommunication Union. *Spectral grids for WDM applications: DWDM frequency grid , ITU-T G.694.1*. Feb. 2012.

[7] M. P. Wartak. *Computational Photonics*. Cambridge University Press, 2013.

[8] International Telecommunication Union. *Spectral grids for WDM applications: CWDM wavelength grid, ITU-T G.694.2*. Dec. 2003.

[9] C. Cole. "100GE SMF WDM Grid Q&A". In: *IEEE 802.3ba Task Force* (Mar. 2008).

[10] C. Chen. *Foundations for Guided-Wave Optics*. Wiley, 2006.

[11] L. A. Coldren, S. W. Corzine, and M. L. Mašanović. *Diode Lasers and Photonic Integrated Circuits*. John Wiley & Sons, Inc., 2012, pp. 451–507.

[12] C. Yeh and F. I. Shimabukuro. *The essence of dielectric waveguides*. Springer, 2008.

[13] E. A. J. Marcatili. "Dielectric rectangular waveguide and directional coupler for integrated optics". In: *The Bell System Technical Journal* 48.7 (Sept. 1969), pp. 2071–2102.

[14] J. Joannopoulos, S. Johnson, J. Winn, and R. Meade. *Photonic Crystals: Molding the Flow of Light*. Princeton University Press, 2011.

[15] P. Yeh and H. F. Taylor. "Contradirectional frequency-selective couplers for guided-wave optics". In: *Appl. Opt.* 19.16 (Aug. 1980), pp. 2848–2855.

[16] P. J. Bock, P. Cheben, J. H. Schmid, J. Lapointe, A. Delâge, S. Janz, G. C. Aers, D.-X. Xu, A. Densmore, and T. J. Hall. "Subwavelength grating periodic structures in silicon-on-insulator: a new type of microphotonic waveguide". In: *Opt. Express* 18.19 (Sept. 2010), pp. 20251–20262.

[17] Y. Shibata, T. Tamamura, S. Oku, and Y. Kondo. "Coupling coefficient modulation of waveguide grating using sampled grating". In: *IEEE photonics technology letters* 6.10 (1994), pp. 1222–1224.

[18] P. Cheben, P. J. Bock, J. H. Schmid, J. Lapointe, S. Janz, D.-X. Xu, A. Densmore, A. Delâge, B. Lamontagne, and T. J. Hall. "Refractive index engineering with subwavelength gratings for efficient microphotonic couplers and planar waveguide multiplexers". In: *Opt. Lett.* 35.15 (Aug. 2010), pp. 2526–2528.

[19] J.-P. Weber. "Spectral characteristics of coupled-waveguide Bragg-reflection tunable optical filter". In: *IEE Proceedings J (Optoelectronics)* 140.5 (1993), pp. 275–284.

[20] C. Riziotis and M. N. Zervas. "Design considerations in optical add/drop multiplexers based on grating-assisted null couplers". In: *Journal of Lightwave Technology* 19.1 (2001), pp. 92–104.

[21] Lumerical. *Lumerical's 2.5D FDTD Propagation Method*. URL: https://www.lumerical.com/support/whitepaper/2.5d_fdtd_propagation_method.html.

[22] R. Halir, P. J. Bock, P. Cheben, A. Ortega-Moñux, C. Alonso-Ramos, J. H. Schmid, J. Lapointe, D.-X. Xu, J. G. Wangüemert-Pérez, Í. Molina-Fernández, and S. Janz. "Waveguide sub-wavelength structures: a review of principles and applications". In: *Laser and Photonics Reviews* 9.1 (2015), pp. 25–49.

[23] F. Horst, W. M. Green, S. Assefa, S. M. Shank, Y. A. Vlasov, and B. J. Offrein. "Cascaded Mach-Zehnder wavelength filters in silicon photonics for low loss and flat pass-band WDM (de-)multiplexing". In: *Opt. Express* 21.10 (May 2013), pp. 11652–11658.

[24] E. L. Wooten, K. M. Kissa, A. Yi-Yan, E. J. Murphy, D. A. Lafaw, P. F. Hallemeier, D. Maack, D. V. Attanasio, D. J. Fritz, G. J. McBrien, and D. E. Bossi. "A review of lithium niobate modulators for fiber-optic communications systems". In: *IEEE Journal of Selected Topics in Quantum Electronics* 6.1 (Jan. 2000), pp. 69–82.

[25] B. Jalali and S. Fathpour. "Silicon Photonics". In: *Journal of Lightwave Technology* 24.12 (Dec. 2006), pp. 4600–4615.

[26] H. A. Haus and W. Huang. "Coupled-mode theory". In: *Proceedings of the IEEE* 79.10 (Oct. 1991), pp. 1505–1518.

[27] A. Yariv. "Coupled-mode theory for guided-wave optics". In: *IEEE Journal of Quantum Electronics* 9.9 (Sept. 1973), pp. 919–933.

[28] A. Lupu, A. Carenco, P. Win, H. Sik, P. Boulet, M. Carre, and S. Slempkes. "Spectral response apodization of Bragg-like optical filters with a novel grating chirp design". In: *Optical Fiber Communication Conference, 1999, and the International Conference on Integrated Optics and Optical Fiber Communication. OFC/IOOC'99. Technical Digest.* Vol. 2. IEEE. 1999, pp. 271–273.

[29] H. Sakata. “Sidelobe suppression in grating-assisted wavelength-selective couplers”. In: *Optics letters* 17.7 (1992), pp. 463–465.